

3 Viscoplastic Impact Modelling

3.1 Introduction

The interest in this chapter is on how to model impacts in space, using a method which shall describe the interaction between different materials, compliant and non-compliant, retaining a high level of fidelity. The answer to this question is important, because a well-established model is necessary for the accurate representation of impacts on simulations. As in Sec. 1.4.1 has been already explained, the impacts can be modelled via three methods: the stereomechanical theory method, the Finite Element Method (FEM) and the compliant/viscoelastic approach. Each method has its pros and cons but the use of the viscoelastic method seems more appropriate, as the impact between different materials can be described by lumped parameter models with suitable characteristics, [145]. There are various models in the literature with more prominent the Hunt-Crossley (HC) model, [76]; in fact the majority of the viscoelastic models use the HC model as a basis and will be also the basis for this work; however this is just a matter of choice. The HC model of Sec. 2.2.4, is repeated here. It is reminded that the interaction force F_g is,

$$F_g(y_g, \dot{y}_g) = k_g \cdot y_g^n + b_g \cdot \dot{y}_g \cdot y_g^n \quad (58)$$

In **Figure 3-1** the shape of a typical HC impact is given. The area inside the curve is the non-recoverable energy which is dissipated during the impact inside the materials under impact, due to mechanisms like internal vibrations and local plastic deformations.

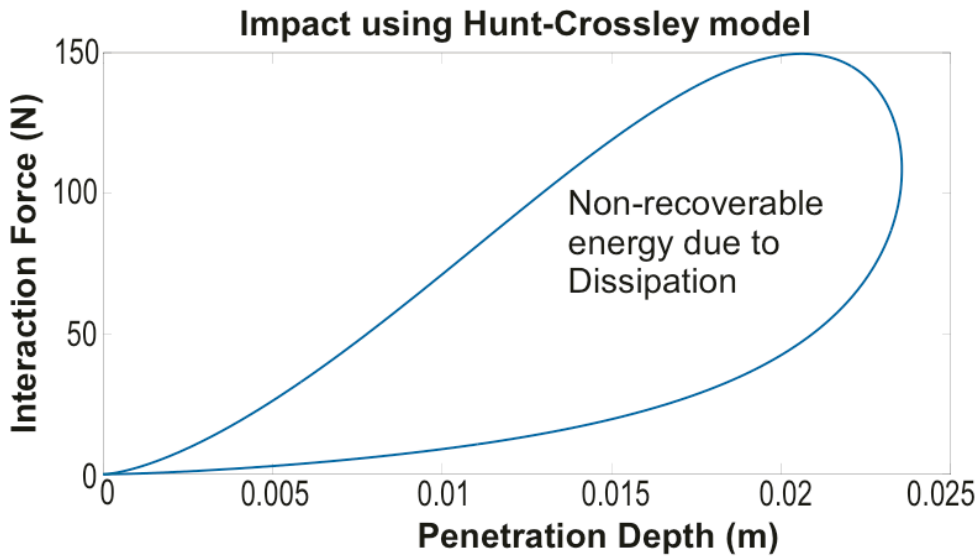


Figure 3-1. Typical Interaction Force – Penetration Depth diagram using HC method.

However, the behaviour of real materials is somehow different according to the experimental results in the literature. In **Figure 3-2** - **Figure 3-4** the experimental results for force vs penetration depth is given for various materials and surfaces. In the case of **Figure 3-2** the pressure is static due to the Bevameter measurement technique. Therefore after each restitution, the compression phase follows almost the previous restitution phase. However it is obvious that the surface due to compaction retains a permanent depth and it does not return to its initial height. During the second pressurization phase (BCD) the materials deform almost from the depth the first pressurization phase ended. Thus the interaction on deformable terrains cannot be represented realistically by methods like HC. The problem is that in a terramechanics approach, like when describing the behaviour of a surface using the Bevameter technique, it is assumed that an equipment (or a wheel or a foot) is in touch with the ground for considerable amount of time, or even permanently. This approach cannot be applied in the case of impacts which are inherently fast. It is reasonable to assume that during impacts, time dependent phenomena, such as creepage, have negligible effect compared to the inertia and interface stiffness or damping effects. However the plastic deformations, which occur to one or both of the interacting bodies, play an important role.

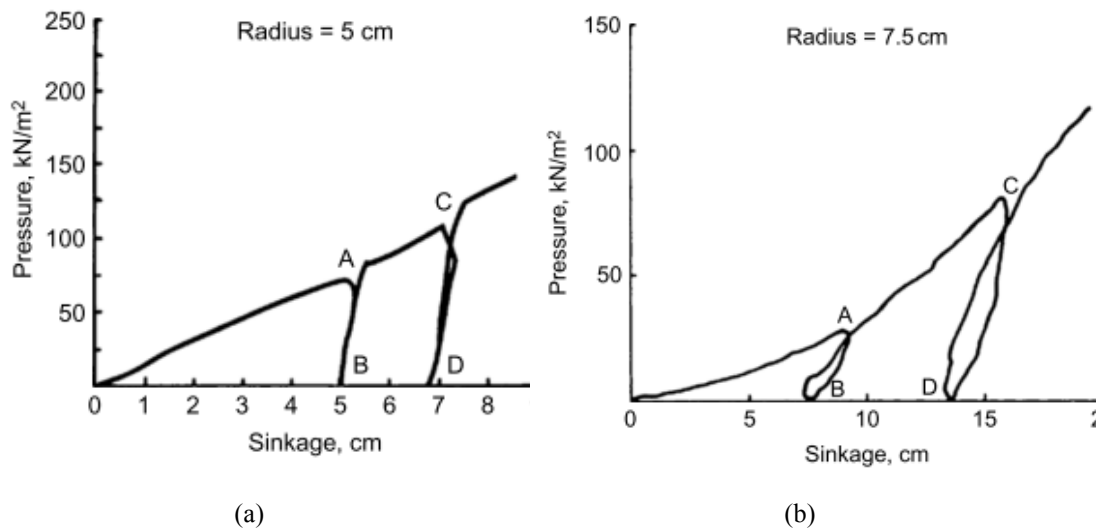


Figure 3-2. Response to repetitive normal load of (a) a mineral terrain, and (b) Petawawa Muskeg A, [162].

In **Figure 3-3** the experimental results of the impact of a metallic sphere on various materials are shown. Again the qualitative similarity of the HC model is apparent, however the HC model fails to predict the permanent deformation analytically. Finally in **Figure 3-4**, the force-penetration depth of a foot (a two-body system) is presented where a recompression phase is acknowledged [83]. However this phenomenon is only observed but not described analytically in that work.

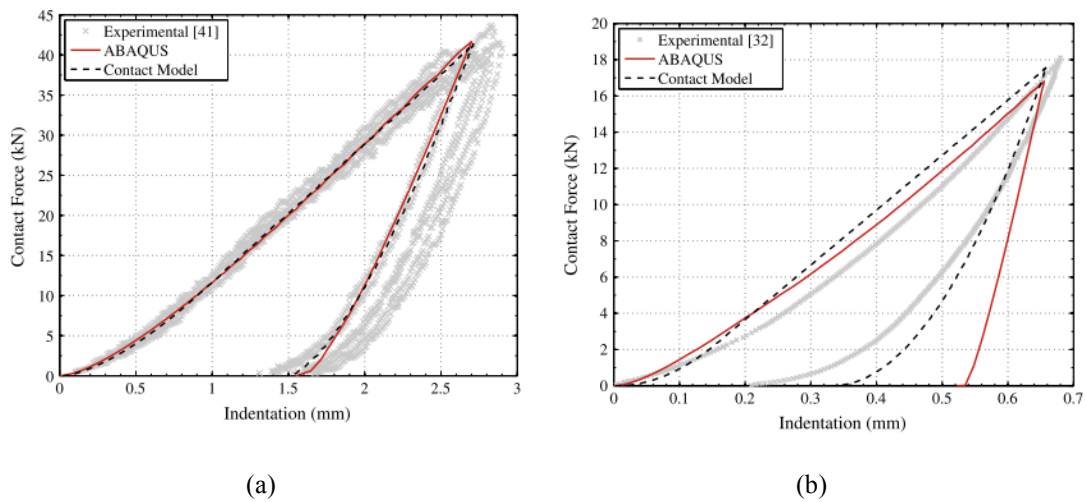


Figure 3-3. Force-Indentation Response of a metallic sphere impacting a (a) composite half-space and (b) rigidly supported thin laminate, [101].

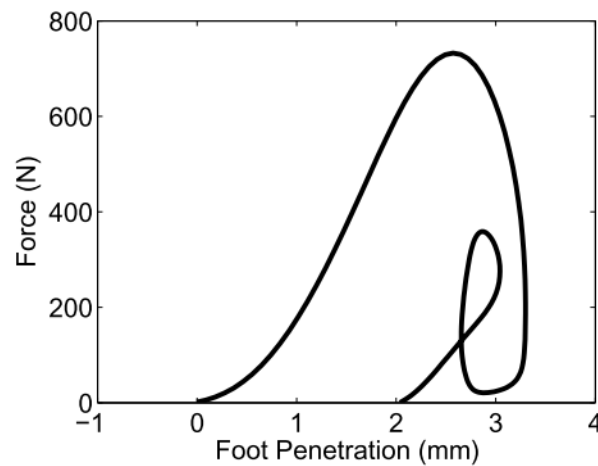


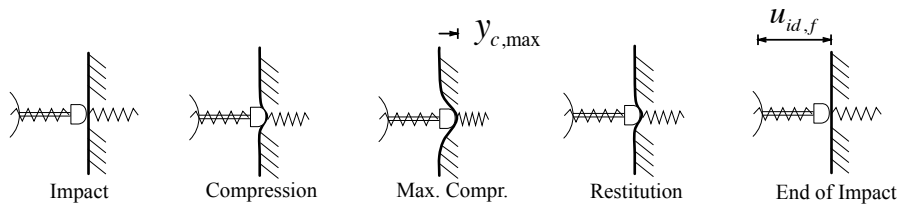
Figure 3-4. Experimental result of a two-body system penetrating a surface (foot-terrain interaction), [83].

In order to tackle the issues that other impact descriptions have, in this chapter a novel impact model is proposed and developed which has viscoplastic characteristics. This viscoplastic model shows very good correlation with experimental results found in the literature and it can efficiently describe a large number of interactions that occur in robotics, not only in space but also in terrestrial applications. At the same time a parameter named *Coefficient of Permanent Deformation* has been introduced, which describes the deformations that can occur on a viscoplastic material, taking into account complex behaviours like compaction and cratering. An earlier work which employs the demonstrated approach in this work and its potential is in [92]. It has been proved that the proposed viscoplastic model represents more accurately this kind of interactions and the generality of its application in viscoplastic impacts applies not only in impacts in space but it can be used similarly in other areas of robotics, [154] - [156].

3.2 Model Rationale

In *viscoelastic models*, in order to describe an impact, lumped parameters (fictional springs and dampers) are used which are located in the interface between the bodies under impact. Let an impact between two bodies, which is defined by a viscoelastic model, such as the HC, **Figure 3-5a**. During compression, both the interaction force F_g and penetration depth y_g increases, while the relative velocity \dot{y}_g between the bodies decreases. When this velocity is zeroed, i.e. $\dot{y}_g = 0$, the maximum compression $y_{c,max}$ has been reached. Note that generally, the maximum force appears before the maximum compression due to intrinsic model non-linearity, [145]. During restitution, the relative velocity between the bodies increases, but in the opposite direction, while the depth and the interaction force decrease. The restitution ends when both the depth and the interaction force are zeroed, but in fact this is due to the closed form of the models. *The key event characterizing the end of the impact is that the interaction force is zeroed, i.e. there is no more contact between the impacting bodies.* In other words, existing viscoelastic models implicitly assume that the impact starts and ends (e) at $y_g = y_e = 0$, i.e. that no permanent deformation $y_e \neq 0$ occurs. However, due to the permanent deformation on a nonideal deformable impact interface, the impact bodies clear the interface at $y_e > 0$; this has an effect on the final elongation of the (fictitious) spring and the energy lost due to the permanent deformation. In addition, in viscoelastic models, the behavior of a material under repetitive loading at the same point, or compaction, is ignored. In fact, experimental results as for example in [29], reveal that viscoelastic models do not describe accurately deformation of materials in contact, validating this proposition. Hence a model that takes into account such deformations is needed.

(a) Impact Using Common Viscoelastic Models



(b) Impact Using Proposed Viscoplastic Model

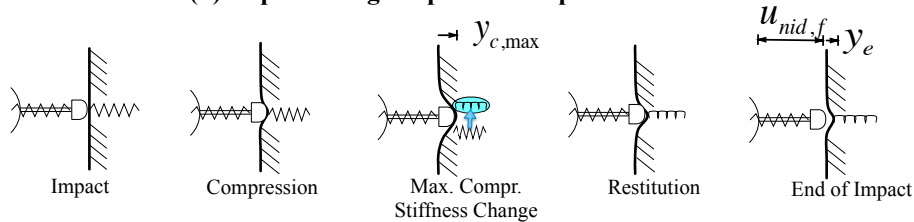


Figure 3-5. Impact models (a) Standard viscoelastic and (b) Proposed viscoplastic.

The strict viscoelastic description of the process can be extended in the case of plastic deformations via appropriate lumped elements to result in a *viscoplastic* description. Here, a model that treats the impact piecewise is developed, as shown in **Figure 3-5b**. According to this model, the compression phase is the same to that in the viscoelastic case. During this phase, part of the energy is stored in the (fictitious) spring, which represents the interaction stiffness, another part is dissipated through material internal losses represented by damping b_g , and the remainder is dissipated during bodies' shape deformation, e.g. due to cratering around the impact point or compaction. As restitution is reached, the material in the direction of motion has been displaced due to the deformation, and/or the interface becomes stiffer because of compaction. Also, the interaction spring cannot be extended to its initial length, corresponding to $y_e = 0$, but to a shorter length corresponding to a new lower level with $y_e > 0$ with respect to the undeformed interface. As the interaction force will be zero at this new free length of the spring, it follows that this new fictitious spring is shorter and stiffer. Thus there is memory for the phase between compression and restitution; this memory will be described by a piecewise equation.

3.3 Proposed viscoplastic model.

In order to mathematically describe the model it is necessary to define the term *impact instance*. An impact, as it has been already presented in Sec. 2.2, is a process which includes the phases of compression (c) and restitution (r), which occur at an impact point. Each pair of compression and restitution on the same impact point is an impact instance. Strictly speaking, an impact terminates when there is no contact between the bodies under impact, thus when the interaction force $F_g = 0$. Therefore an impact may consist by one or more compression-restitution pairs until it is terminated; thus an impact may consist by one or more impact instances.

Based on the above, the interaction force F_g at an impact instance i can be described by,

$$F_{g,i}(y_g, \dot{y}_g) = \begin{cases} F_{c,i} = (\lambda_{c,i} \cdot k_g + b_g \cdot \dot{y}_g)(y_g - y_{e,i-1})^n, & \dot{y}_g \geq 0 \\ F_{r,i} = (\lambda_{r,i} \cdot k_g + b_g \cdot \dot{y}_g)(y_g - y_{e,i})^n, & \dot{y}_g < 0 \end{cases} \quad (59)$$

where subscript c stands for compression, r for restitution, y_e is the final penetration depth, and the index i identifies the impact instance, see **Figure 3-5**. As the interface between the bodies under impact inherits characteristics from the previous instance, during successive impacts at the same point, the *Coefficient of Permanent Deformation* λ is defined in recursive form as,

$$\lambda_{c,i} = \begin{cases} 1, & i=1 \\ \lambda_{r,i-1}, & i>1, i \in \mathbb{N} \end{cases} \quad (60)$$

$$\lambda_{r,i} = \lambda_{r,i}(\text{materials, velocity, } i), \quad i \in \mathbb{N}$$

Since the fictitious spring is stiffer during restitution than in compression, $\lambda_{r,i} \geq \lambda_{c,i} \geq 1$. The equality $\lambda_{r,i} = \lambda_{c,i}$ holds when the interface cannot be compressed further; then (59) reduces to an HC model with the same start and end point. As a demonstration, **Figure 3-6** illustrates the impact force as a function of the penetration depth y_g for various fixed values of λ as described by (59), in the case of a 1kg ball falling with zero velocity from a 0.5m height to a surface with $k_g = 8 \cdot 10^4$ N/m. Note that with λ increasing, the permanent deformation increases, even though the compression phase is the same. The area under the curve corresponds to interaction losses; these increase with λ . In **Figure 3-7**, the distribution of the energy dissipation is presented. The areas below the two HC curves (compression and restitution) represent the dissipation due to internal losses, as in **Figure 3-1**. The triangled-shaped area, of which the sides are described by the non-linear springs of each phase in (59), represents the energy loss due to the permanent shape deformations.

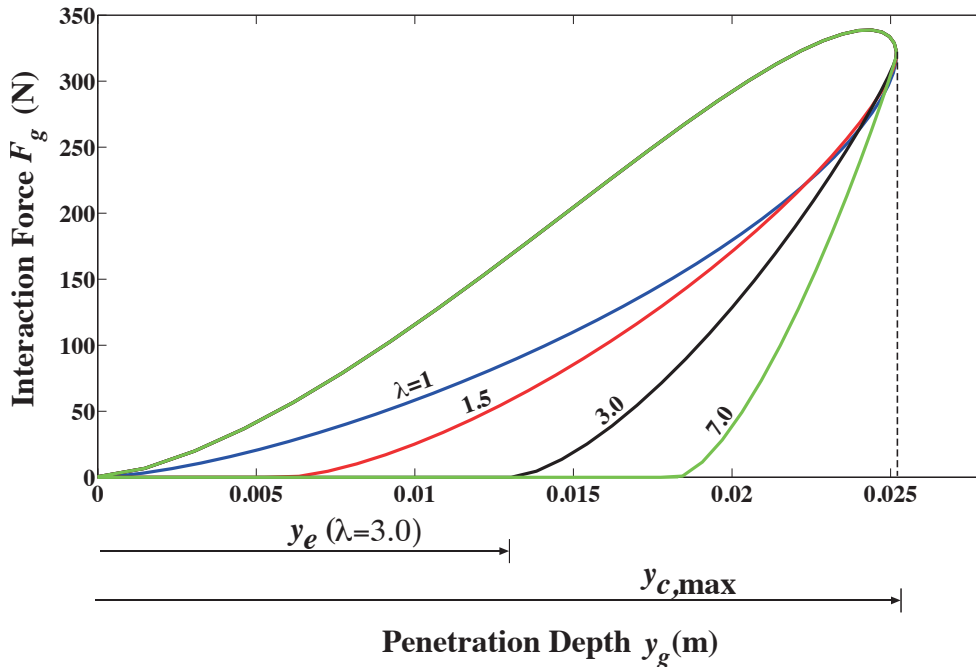


Figure 3-6. Impact curves for the proposed impact model (59) for various λ .

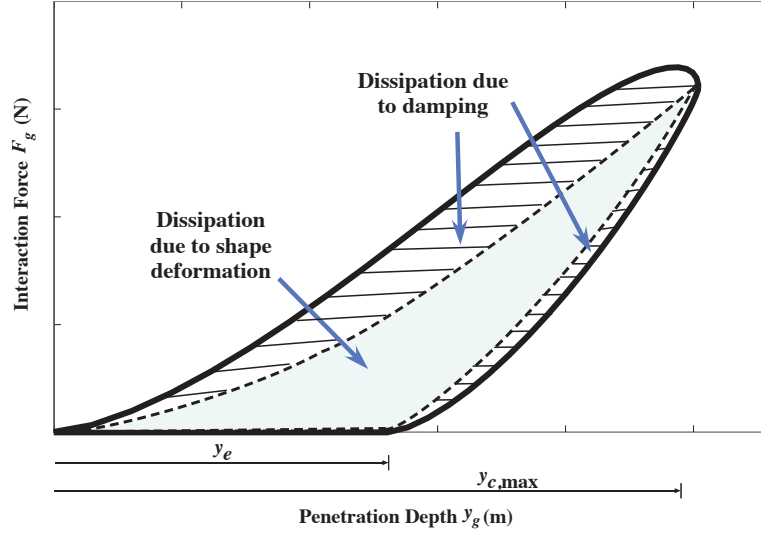


Figure 3-7. Energy dissipation as depicted in the impact curve.

Parameters for various materials or soils can be obtained easily from the literature, e.g. [29], [58] and [71]. However, usually the experiments that yield these parameters are of static nature, e.g. for soils this is achieved using the Bevameter technique (such as the cohesion), which may not be adequate for dynamic impacts.

Generally, as the same contact area is compressed, it becomes stiffer. Thus after a number of impacts at the same point, its stiffness eventually reaches a critical limit. To model this increasing stiffness, the following function is proposed,

$$\lambda_{r,i} = 1 + a(i) \cdot (1 - e^{-i\beta(i)}), \quad i \in \mathbb{N} \quad (61)$$

where $a(i)$ and $\beta(i)$ are functions of the impact instance i , of the materials and of the velocity. Note that if $a(i) = 0$ or $\beta(i) = 0$, (59) reduces to the HC model. Parameter a sets the maximum value of $\lambda_{r,i}$, whereas an increase in β increases the speed to reach this value, i.e. fewer impacts at the same point are needed to reach the critical value, as shown in **Figure 3-8**. Apparently as the impact instance is a discrete value, $\lambda_{r,i}$ has also discrete values.

The final depth $y_{e,i}$ after the i^{th} impact can be calculated by observing that at the maximum compression $y_{c,\max,i}$ there is force continuity, while the interface velocity is zero, i.e.

$$y_{c,\max,i} \Leftrightarrow F_{c,i} = F_{r,i} \quad \text{and} \quad \dot{y}_g = 0 \quad (62)$$

Using (59) and (62) one can deduce that

$$y_{e,i} = y_{c,\max,i} \cdot \left(1 - \sqrt[n]{\lambda_{c,i}/\lambda_{r,i}}\right) + y_{e,i-1} \cdot \left(\sqrt[n]{\lambda_{c,i}/\lambda_{r,i}}\right) \quad (63)$$

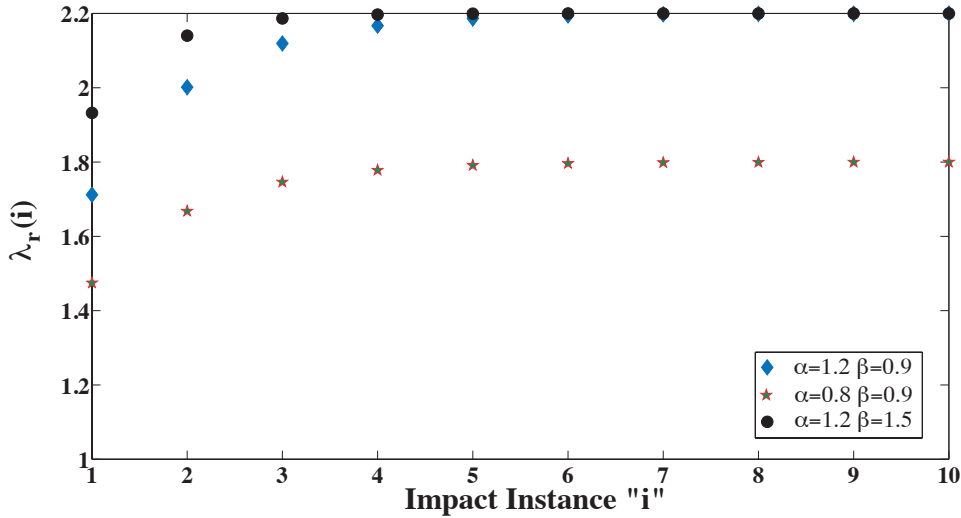


Figure 3-8. Change of the Coefficient of Permanent Deformation after each impact using (61) for various $a(i)$ and $\beta(i)$. The values are discrete.

where $y_{e,0} = 0$ for consistency.

3.4 Recompressions, rebounds, and hard impacts.

It is interesting to study the impact behavior of the two-body system in **Figure 3-9**, while it falls vertically (it has the same behaviour with a system which hits horizontally another system or wall) where the lower mass is lighter than the upper mass. When the lower mass comes into contact with the interface, the direction of the velocity of the system CoM is downward. The phases of compression and restitution occur, **Figure 3-9a** and **Figure 3-9b**; during restitution the lower mass may or may not clear the interface, **Figure 3-9c**. However the upper mass due to its larger inertia and system compliance, continues its downward motion and thus the forces which are applied on the lower mass by the spring (and damper) and the interface interaction can become equal in magnitude before the direction of the velocity of the system CoM is reversed. This will start a "recompression" phase (impact instance $i+1$ for this interface point), **Figure 3-9d**. The process can be repeated a number of times until the two-body system as a whole clears the interface and at the same time the direction of the velocity of the system CoM becomes upward; only then the impact is considered over.

Therefore the possible cases during an impact of the two-body system of **Figure 3-9** are:

i) After the i^{st} restitution, m has cleared the interaction surface (whether it is the initial depth or a surface compressed to $y_{e,i}$) and its velocity is upward. Thus $F_g = 0$. If the CoM of the system continues its downward motion, the phenomenon is a rebound. Another impact instance $i+1$ will take place.

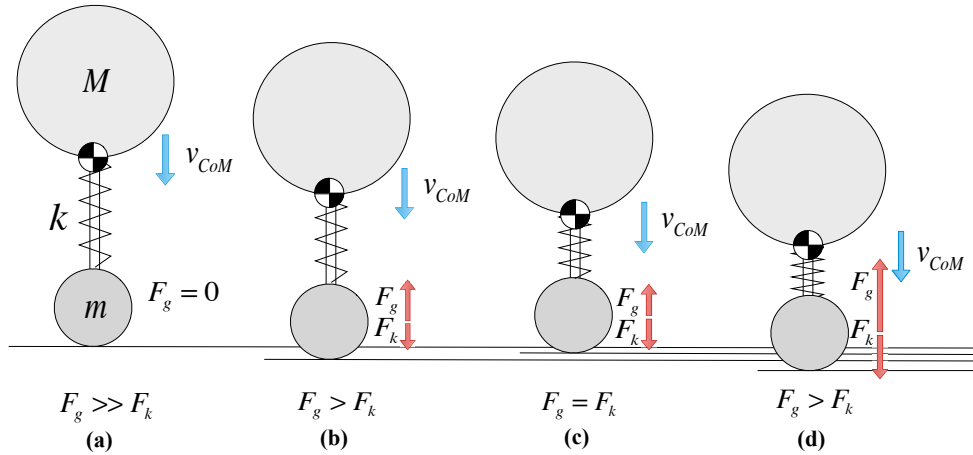


Figure 3-9. Description of recompression for a falling 2-body system where F_g is the interaction force and F_k is the spring force: (a) Initial contact, (b) Compression, (c) Restitution and (d) Recompression.

- ii) After the i^{st} restitution, m has not cleared the interaction surface (whether it is the initial depth or a surface compressed to $y_{e,i}$). Thus $F_g \neq 0$ and the CoM of the system continues its downward motion. In this case the phenomenon is a recompression. Another impact instance $i + 1$ will take place.
- iii) After the i^{st} restitution, m has cleared the interaction surface (whether it is the initial depth or a surface compressed to $y_{e,i}$) and its velocity is upward. Thus $F_g = 0$. If the CoM of the system has also an upward motion, the impact has been terminated. No other impact instance will take place.

As an application of this behaviour, the interaction force versus the penetration depth is presented in **Figure 3-10** for a two-body system which impacts a very stiff ground ($k_g = 10^6 \text{ N/m}$), where the upper and lower masses are 4 kg and 0.1 kg respectively, the distance between them is 0.30 m and the spring stiffness is $k = 12,000 \text{ N/m}$. For demonstration purposes, (61) is used with $a = 0.5$ and $\beta = 1$, corresponding to a very stiff surface, which can be deformed plastically to some small degree. The system falls from a height of 1 cm with zero initial velocity. As it can be seen in **Figure 3-10**, a number of compression and restitution phases are observed before the interaction force is zeroed. The remaining compression is about 0.45 mm.

On the other hand, a *rebound* is completed when the lower mass clears the ground; more than one rebounds can occur during a single impact phase. **Figure 3-11** illustrates the characteristic behavior for two different impacts. In the first impact, the lower body undergoes a number of successive recompressions, without clearing the surface; thus no rebound occurs. In the second

impact, clear of the surface by the lower body occurs, but the velocity direction of the CoM is opposite to the velocity direction of the lower mass; thus a rebound occurs.

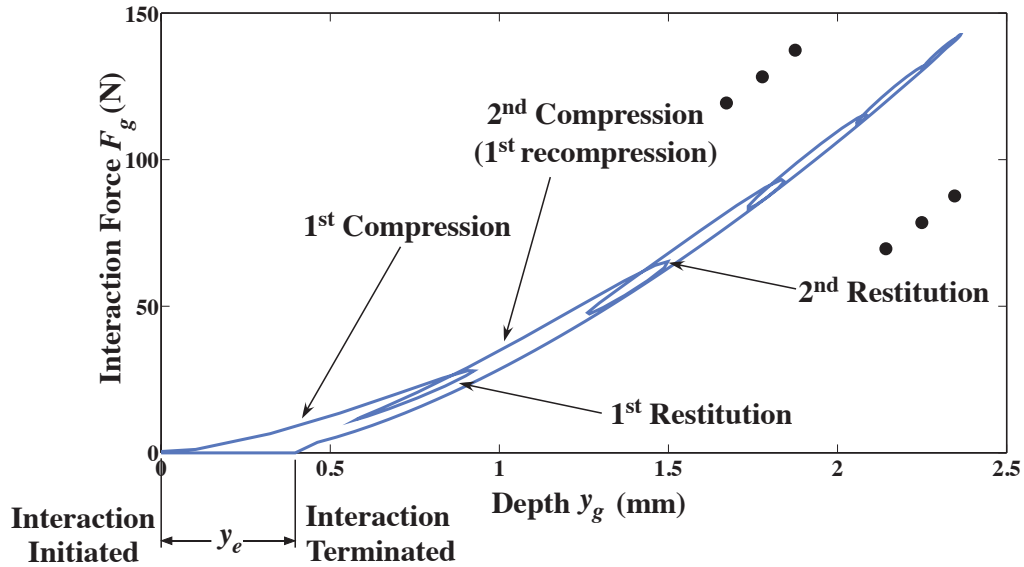


Figure 3-10. Impact curve for a case with 5 recompressions.

The observations are very interesting for a robotic system, as for example in the case of foot-terrain interaction. A force sensor is used often in legged robots to establish the transition from stance to flight and vice versa, so it is possible that the sensor signals can mislead the controller; therefore this behavior must be taken into account in the controller design. Otherwise, flight and stance controllers will be switched on and off very fast, resulting in poor response or even in eventual loss of stability, especially when the impacts are between stiff bodies, [102].

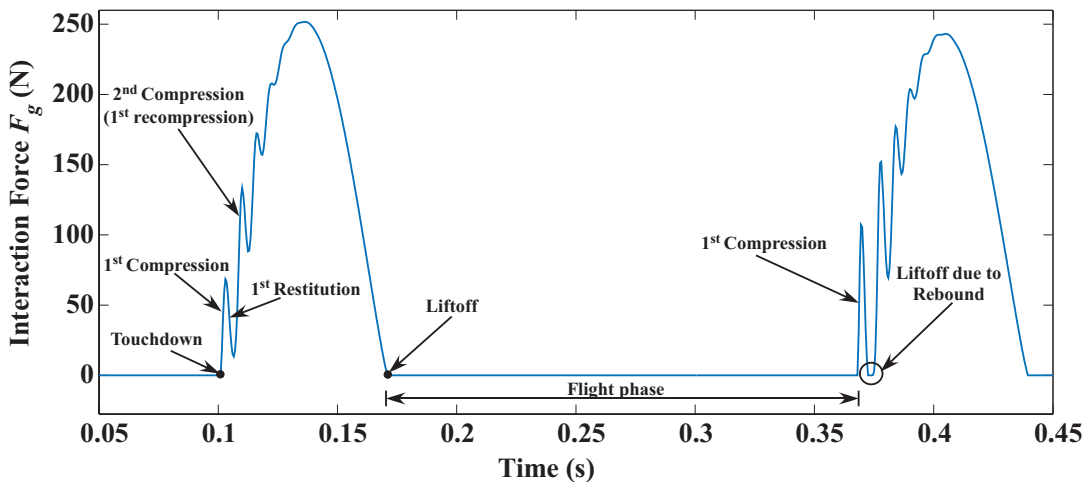


Figure 3-11. Stance instances with recompressions and rebounds.

3.5 Discussion on the proposed viscoplastic model

Let now examine the qualitative results of using the proposed viscoplastic model. Let again the case of a 1kg ball falling to a surface with $k_g = 8 \cdot 10^4 \text{ N/m}$, but this time the velocity just prior to impact is 2 m/s and this time the interaction damping characteristics and the Coefficient of Permanent Deformation λ are changing, **Figure 3-12**. As the damping characteristics are relatively low, and the Coefficient of Permanent Deformation is unity, the absolute velocity after restitution is almost equal to the absolute velocity before the impact; the impact is almost elastic. By increasing the damping characteristics of the surface – that is the dissipation due to damping is increased – the absolute velocity is reduced. Using (9), it is easy to determine the coefficient of restitution equal to 0.475. However when the damping characteristic is retained but the Coefficient of Permanent Deformation is increased the behaviour is different; the compression phase is similar to the previous one but the impact finishes earlier, and the final velocity is reduced further. The coefficient of restitution can be calculated again by (9) equal to 0.275; energy has been dissipated not only in the interior of the surface, but also the plastic deformation (designated by the Coefficient of Permanent Deformation) reduced further the ball's final velocity.

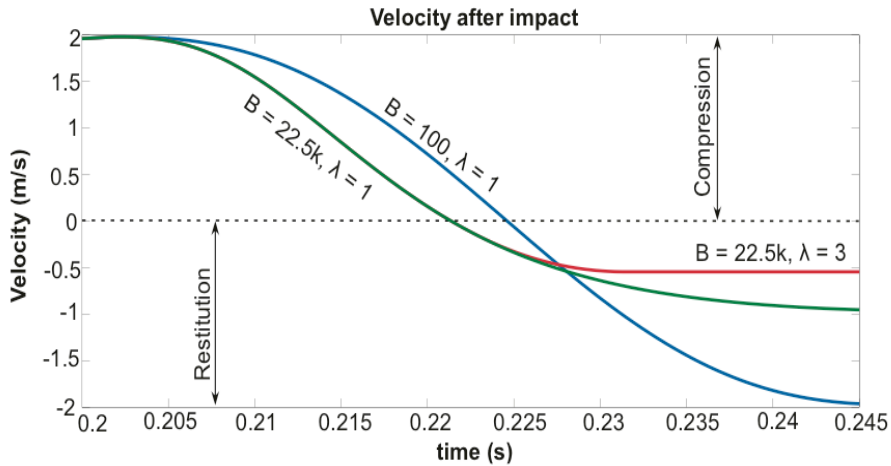


Figure 3-12. Qualitative difference between viscoelastic model and proposed viscoplastic model.

Note that in any case, the actual penetration depth as a function of the interaction force depends not only on the materials and the initial impact velocity, but also on the relative stiffness of the system with respect to the surface and the system mass ratio.

Summarizing, the proposed model:

(a) has advantages over similar models like KV, HC, or those presented in [6], [82], [83], [162]. The model can both describe accurately the impact between two compliant bodies but it can also be used for repetitive loading of a particular contact point by increasing the impact instance

index i for this particular contact point. A special case of repetitive loading occurs when the impacting body is a multibody system where recompression may occur,

(b) is numerically stiff. Depending on the complexity of the problem to solve, high accuracy in ODE solvers may be required,

(c) uses the HC model as a basis in (59), but this is purely a matter of choice; the core idea of the developed model is also applicable to other viscoelastic models,

(d) proper selection of λ can describe complex interaction phenomena like compaction and cratering, and.

(e) experimental results in the literature, prove that the proposed model has qualitatively similar results, see Sec. 3.1. The exact figures for the stiffness/damping characteristics of many materials and surfaces can be found in the literature, like in [101] and [162].

The pseudocode of the algorithm of the impact model can be found in **Appendix D**.

4 Analyzing Impacts Between Multibody Systems

4.1 Introduction

In this chapter the interest lies on how the mass and stiffness characteristics of systems under impact affect the impact in a gravity-free (zero gravity) environment. Initially, the standard approach during modeling of impact docking is presented and it is shown that this approach lacks on accounting the effects of inertia and stiffness of the system of masses that come into contact. A more generalized approach in modeling this free-floating impact by using computationally fast methods stemming from the rigid-body theory is developed. One important result here is that the effect of the mass ratio of the multibody systems under impact is quantified. This quantification is achieved using an analytical proof of the effect of mass ratios during impact of multibody systems. This resulted to a better understanding on the behaviour of multibody systems in zero-gravity during impacts. In line with this, the *Ratio of Effective Masses* is introduced, which can efficiently describe the behaviour of multibody systems under impact, taking into account all the masses of the impact. By using this term, a fast but accurate way to assess the post-impact relative velocity knowing only the pre-impact relative velocity is presented. Additionally using this ratio, it can be determined whether the impact of two systems can lead to a further approach or separation. Thus, in this chapter, an analytical method for fast determination of the behaviour of multibody systems under impact is developed and it is used in order to define whether the conditions for a successful docking/ capture exist. Part of this work has been presented in [126].

4.2 Model Development

4.2.1 Discussion on Models to Describe Impact Docking

Usually the model used for the impact during docking is 1-D due to the fact that the salient information of the impact can be described in this way, [35], see **Figure 4-1**. The problem with this model is the fact that on part of the system, or for both systems, one or more bodies can be replaced by a fictional wall. This is near the reality if and only if a body has a very large mass comparing to the others. For example this model is near to reality in case the Target is the ISS. However as the bodies under impact have comparable masses, this simple model fails to represent the reality. This is especially true if we consider impacts during docking between satellites (e.g. in a on-orbit servicing scenario) or the capturing of a space debris by a space robot.

A more generic model for the Chaser and the Target CoMs when moving along the same axis is shown in **Figure 4-2**. Both systems are modelled as two masses connected with a (in general non-linear) spring and a (in general non-linear) damper. This may seem as an

oversimplification, especially when the Chaser, the Target or both, are n-body systems; however according to the assumptions of Sec. 2.2.2, during the short duration of an impact, the systems can be regarded as *quasi-static*. In this approach, it can be regarded that the Chaser is a combination of a mass which resembles the base and some of the links which have locked joints or very high stiffness comparable to a joint which connect a probe (and perhaps some more links), which are the mass. In a similar way the Target, can be regarded as one base with a latching mechanism (or drogue), connected via a spring and a damper. In other words, what interest is the first eigenfrequency that corresponds to two masses and a spring for each system, Chaser and Target.

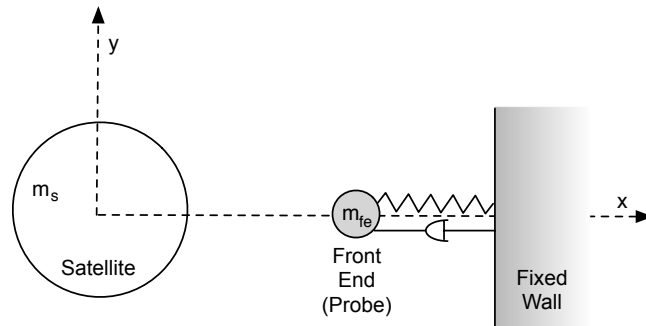


Figure 4-1. Classic modelling of docking impact procedure.

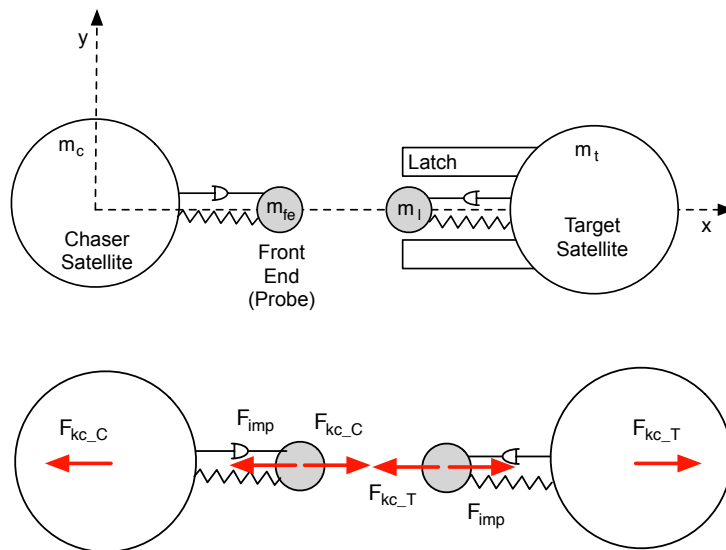


Figure 4-2. Generic model of impact between two free-floating systems.

Specifically, if the free body diagram is analyzed, one can see the main equations of motions for all masses of this system. Unfortunately, the absence of a fictitious wall as in the classic analysis, makes the problem more difficult to analyze. In order to select the proper model for the docking impact, it is necessary to discuss the parameter of the model to pinpoint its characteristics. In this

discussion the 1-D models shall be examined, as they form the basis for any subsequent analysis in 2-D or 3-D:

4.2.2 Discussion on the Stiffness Characteristics

In many cases in the literature, it is usual to consider the probe front-end as a small mass, which is ignored. However this is not realistic: As the front-end comes into contact with the Target, the impact occurs between these two bodies (the small mass and the target). Higher impact frequencies are excited than in the case in which the small mass is neglected. Thus the masses cannot be simply ignored, as in reality they are the main reason for energy interaction between the Chaser and the Target. Therefore a question is eminent: which is the mass ratio that defines the model to be used during impacts?

As Stronge and other researchers suggest [145], when there are multiple impacts between multiple masses, like in the case of the 2 two-bodies we examine, the ratio between the spring constants between the masses and the spring constant which represents the interaction between the bodies under impact play an important role. On main issue which arises, is whether the impacts can be considered sequential or simultaneous. Generally, if the magnitude of the spring constant which represents the impact is much higher than the spring constants between the bodies of the Chaser and the Target, the impacts are simultaneous. In more detail, as the ratio of the impact stiffness to the internal stiffness of the bodies is larger than one order of magnitude, the impact characteristics (maximum force, duration) are governed by the stiffer spring, which in this case is the fictional spring between the masses under impact.

The first question is how realistic is this in the case examined, that is the impact between the 2 two-body systems in space. It is reasonable to assume that the spring constant developed between the bodies under impact, k_i , is far larger than the springs between joints. Indeed, see Sec. 2.2.6, a typical spring constant between two metallic surfaces can be high enough (more than some hundred thousands for this case), whereas a typical spring constant created by a joint (either using a spring or a motor) is much lower – except of course it is a locked joint.

The second question is what happens as the ratio is lower than one order of magnitude. In other words what happens as the spring constants k_i and k_c or k_t , are similar. The following cases exist: (1) The spring constant between the masses of the Chaser and the Target are larger than the fictional spring constant k_i for at least one order of the magnitude. In this case one can consider that the Chaser is two masses rigidly connected. (2) If we remove the masses under impact as very small, then the total spring constant can be evaluated using Eq. (200). In other words we can model again the systems as a two mass system connected with an equivalent spring. (3) In case that all spring constants are of the same order of the magnitude then the viscoelastic

analysis is necessary. However until now an analytical solution is difficult to be found for more than 3 interconnected bodies, and FEM analysis may be necessary. Hopefully this is not a case of interest, as it is completely unrealistic with respect to this problem; the impact is usually between metallic elements, therefore k_i is much larger than k_c or k_t .

4.2.3 An n-multibody system modelled as a 2-body system

The impact docking has mainly to do with systems where the probe-drogue mechanisms are not connected to appendages (e.g. ATV docking on ISS), but in the more general case, it is assumed that they are attached to manipulators, (i.e. configurable appendages). By reference to **Figure 4-3a**, suppose that the probe and drogue are both connected to a manipulator, and each manipulator to a free-floating base. This can be simplified if examined as a 1-D case, see **Figure 4-3b**.

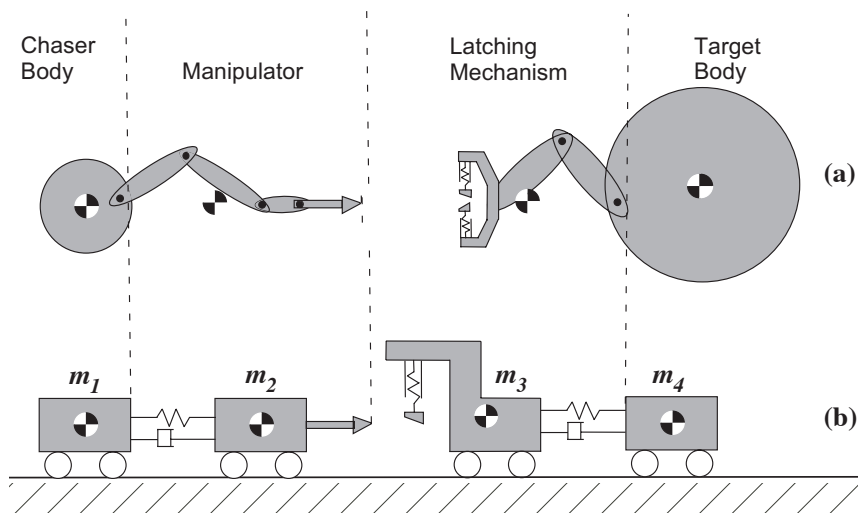


Figure 4-3. Model rationale of impact docking between multibody systems: (a) concept and (b) free body diagram.

With reference to **Figure 4-3b**, the Chaser is a two-body system, where mass, m_1 , represents the Chaser body and mass m_2 , its manipulator with the probe. These are connected via a lumped parameter system, (a spring and a damper), modelling the internal compliance of the system. Similarly for the Target, a system of two masses (m_3 and m_4) connected by lumped parameter elements is employed. Specifically for the 1-D case, the latching mechanism is regarded to be a spring-latch system, which is parallel or normal to the motion of the bodies under impact. This method of modelling is similar to known approaches such as those in [35] and [151]. This is the generic scenario which will be used in this work and is based on the current technology trends of Sections 1.2 and 1.3.

Thus, it is useful to model the multibody systems under impact as 2-body systems; this approach is known as *equivalent two-body system identification*, [164]. That is an “n” multibody

system, under impact, can be modelled as a 2-body system with one body being equivalent to the first k masses, and the second body equivalent to the rest $n-k$ masses, connected by equivalent spring/damper elements. The general case is shown in **Figure 4-4**. Let that a space robot is comprised by a main body, some flexible appendages (e.g. antennas, solar panels) and a robotic manipulator with $n-1$ links. Without introducing large errors, we can ignore the small masses located away from the impact point and introduce a much larger mass in the middle. Additionally the rest of the joints are locked, while a single joint remains able to rotate.

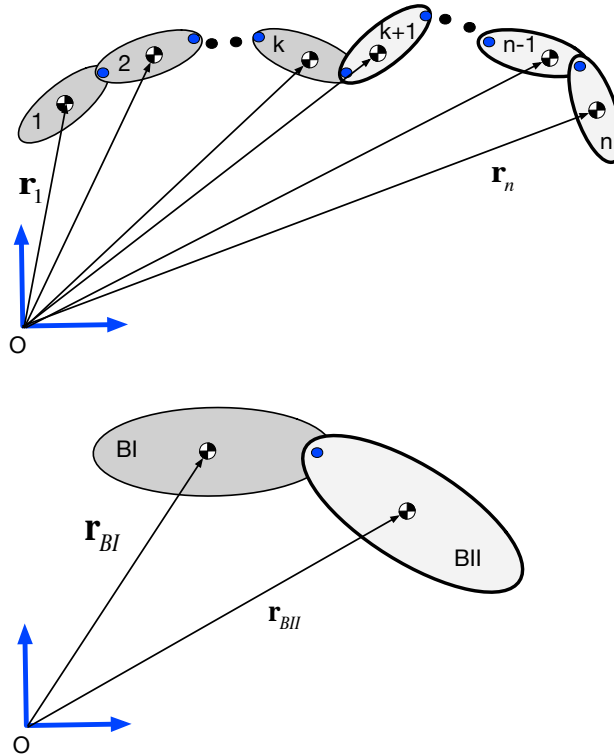


Figure 4-4. Equivalence of a n-body system with a 2-body system.

As it is known from mechanics the inertia characteristics can be calculated. For example the Center of Mass (CoM) of the n-body system is

$$\mathbf{r}_{cm} = \frac{\mathbf{r}_1 \cdot m_1 + \mathbf{r}_2 \cdot m_2 + \dots + \mathbf{r}_k \cdot m_k + \mathbf{r}_{k+1} \cdot m_{k+1} + \dots + \mathbf{r}_{n-1} \cdot m_{n-1} + \mathbf{r}_n \cdot m_n}{m_1 + m_2 + \dots + m_k + m_{k+1} + \dots + m_{n-1} + m_n} \quad (64)$$

The CoM of the 2-body system is

$$\mathbf{r}_{cm} = \frac{\mathbf{r}_{BI} \cdot m_{BI} + \mathbf{r}_{BII} \cdot m_{BII}}{m_{BI} + m_{BII}} \quad (65)$$

therefore

$$m_{BI} \cdot \mathbf{r}_{BI} = \sum_{i=1}^k m_i \cdot \mathbf{r}_i \quad (66)$$

$$m_{BII} \cdot \mathbf{r}_{BII} = \sum_{i=k+1}^n m_i \cdot \mathbf{r}_i \quad (67)$$

By incorporating this methodology it is possible to find an equivalent 2-body system for any multibody system. This will be useful in the next sections in order to determine whether an impact between two 2-body systems can lead to approach or to move away one from another.

4.3 Rigid Multibody Impact Theory

The common multibody impact models use techniques which are by design computationally expensive. Even though novel algorithms and increased computational power exist today, the computation of the impact behaviour of a n-body system takes time and is not favoured for the computer of a space system during operations which include impacts.

For this reason the Rigid Multibody Impact Theory (RMIT) is proposed, [126]. The difference from other multibody impact models is that in this model the bodies are considered as whole systems (Chaser and Target) *and* as separate masses (two masses for the Chaser, two masses for the Target) *simultaneously*, see **Figure 4-5**. The idea behind this concept is based on Sec. 2.3.2. More specifically, let a multibody Chaser system of total mass m_c which can be equivalently substituted by two masses, m_1 and m_2 , connected by a spring k_c and a damper c_c representing the compliance at this point. Similarly, let a multibody Target system of total mass m_t which can be equivalently substituted by two masses, m_3 and m_4 , connected by a spring k_t and a damper c_t representing the compliance at this point. During impact the masses m_2 and m_3 come into contact first. That is the impact characteristics are inevitably connected with these two bodies. However at the same time, the impact occurs between the total masses of the two multibody systems, m_c and m_t which include the masses under impact m_2 and m_3 . *In other words during an impact there is an interaction which exchanges energy between the masses under impact (m_2 and m_3) as well as the total masses (m_c and m_t).* During this analysis it shall be proven, that using equations of classical rigid body impact mechanics, one can predict the behaviour of the total systems after impact without large computational requirements.

Four different effective masses are defined, see also **Appendix A**. More specifically, the effective mass of the total Chaser and Target systems (total system effective mass) is:

$$m_{i,ef} = \frac{m_c \cdot m_t}{m_c + m_t} \quad (68)$$

the effective mass of the bodies under impact (the masses that come first into contact) is

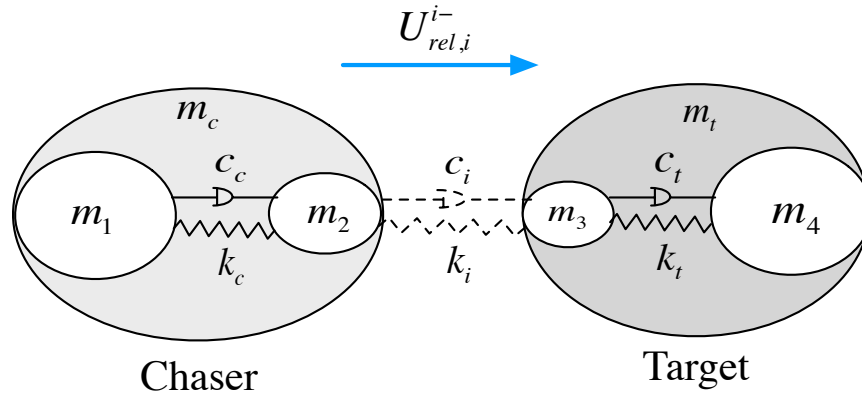


Figure 4-5. Concept for Multibody Contact Model.

$$\mu_{i,ef} = \frac{m_2 \cdot m_3}{m_2 + m_3} \quad (69)$$

and the effective masses of each of the Chaser and Target are

$$\mu_c = \frac{m_1 \cdot m_2}{m_1 + m_2} \quad (70)$$

$$\mu_t = \frac{m_3 \cdot m_4}{m_3 + m_4} \quad (71)$$

Due to the impact instant “i” (see also 3.3 for the definition of the term impact instance), an impulse P_{imp}^i is created, which by using the expression of impulse according to (17) for the model into consideration is

$$P_{imp}^i = (1 + e^*) \cdot U_{rel,i}^- \cdot \mu_{i,ef} \quad (72)$$

where $U_{rel,i}^-$ is the relative velocity of the bodies under impact prior to impact “i”, and e^* is the coefficient of restitution. Note that from now on, when the signs are used in superscripts they have the following meaning: “-” represents a value just prior to impact and “+” represents a value just after the impact. *The same impulse P_{imp}^i is developed between m_2 and m_3 , and between m_c and m_t , [78].* This understanding is critical to the rest of the analysis.

Let now define the relative velocity between the systems $U_{rel,s}^{i\pm}$ before or after impact “i” (according to the sign) as,

$$U_{rel,s}^{i\pm} = V_c^{i\pm} - V_t^{i\pm} \quad (73)$$

where $V_j^{i\pm}$, $j = c, t$ is the absolute velocity of the Chaser (c) or Target (t) before or after impact instant “i” with respect to the same CS. Using (8) one can see that the following relationships apply,

$$P_{imp}^i = m_c \cdot (V_c^{i-} - V_c^{i+}) \quad (74)$$

$$-P_{imp}^i = m_t \cdot (V_t^{i-} - V_t^{i+}) \quad (75)$$

due to action-reaction principle. Therefore the relative velocity of CoMs of Chaser and Target after impact is

$$\begin{aligned} U_{rel,s}^{i+} &= V_c^{i+} - V_t^{i+} = \left(V_c^{i-} - \frac{P_{imp}^i}{m_c} \right) - \left(V_t^{i-} + \frac{P_{imp}^i}{m_t} \right) = (V_c^{i-} - V_t^{i-}) - P_{imp}^i \cdot \left(\frac{1}{m_c} + \frac{1}{m_t} \right) \Rightarrow \\ &\Rightarrow U_{rel,s}^{i+} = U_{rel,s}^{i-} - \frac{P_{imp}^i}{m_{i,ef}} \end{aligned} \quad (76)$$

Using (72)

$$U_{rel,s}^{i+} = U_{rel,s}^{i-} - \frac{P_{imp}^i}{m_{i,ef}} = U_{rel,s}^{i-} - \frac{(1+e^*) \cdot U_{rel,i}^{i-} \cdot \mu_{i,ef}}{m_{i,ef}} \quad (77)$$

Equation (77) shows that the relative velocity between the two multibody systems after impact is related to the relative velocity of the two multibody systems prior to impact, reduced by an amount which is related to the coefficient of restitution, the relative velocity between the bodies under impact (i.e. m_2 and m_3) and the way the masses of all bodies ($m_1, m_2, m_3, m_4, m_c, m_t$) are distributed. It is important that the difference of the two relative velocities $U_{rel,s}^{i-}$ and $U_{rel,i}^{i-}$ is clear: The first refers to the relative velocity of both masses m_c and m_t , and the second refers to the relative velocity of the bodies under impact m_2 and m_3 . Generally these two relative velocities are not the same, for example in the case we examine, if m_2 and/or m_3 are oscillating with respect to their body frame CS{B}. In order for the equation $U_{rel,s}^{i-} = U_{rel,i}^{i-}$ to apply, two cases exist:

- a) There is no internal relative motion between the bodies of Chaser and between the bodies of Target. This means that the Chaser’s masses have the same velocity (and therefore the same velocity with their system CoM), and the Target’s masses have the same velocity (and therefore the same velocity with their system CoM). In the case examined this means that the internal springs of Chaser and Target are at their free lengths. This case is usually reasonable prior to first impact in a nominal approach scenario.

- b) In the case that another impact (i.e. not the first impact) occurs right at the point that both springs are at their free length.

Therefore the relative impact velocity $U_{rel,i}^{i-}$ can be expressed as

$$U_{rel,i}^{i-} = U_{rel,s}^{i-} + \delta U_{rel}^{i-} \quad (78)$$

where δU_{rel}^{i-} is the relative difference of velocities between the impact bodies mass (m_2 and m_3) due to their motion within their systems (here in the form of oscillations), when the relative velocity of the systems has been subtracted. Using (77) and (78) one can find

$$\begin{aligned} U_{rel,s}^{i+} &= U_{rel,s}^{i-} - \frac{P_{imp}^i}{m_{i,ef}} = U_{rel,s}^{i-} - \frac{(1+e^*) \cdot (U_{rel,s}^{i-} + \delta U_{rel}^{i-}) \cdot \mu_{i,ef}}{m_{i,ef}} \Rightarrow \\ &\Rightarrow U_{rel,s}^{i+} = \left(1 - \frac{(1+e^*) \cdot \mu_{i,ef}}{m_{i,ef}} \right) U_{rel,s}^{i-} - \frac{(1+e^*) \cdot \mu_{i,ef}}{m_{i,ef}} \cdot \delta U_{rel}^{i-} \end{aligned} \quad (79)$$

Using the notation e_I for the ratio of effective masses between bodies under impact and total system

$$e_I = \frac{\mu_{i,ef}}{m_{i,ef}} \quad (80)$$

In essence the ratio e_I provides a metric of how much of the energy between two multibody systems is transferred between the bodies which are directly under impact (thus m_2 and m_3) with respect to the energy transferred to the whole systems (thus m_c and m_t), due to their inertia characteristics. Combining with the coefficient of restitution in (79)

$$e_I^* = (1+e^*) \cdot e_I \quad (81)$$

one can write (79) as

$$U_{rel,s}^{i+} = (1-e_I^*) U_{rel,s}^{i-} - e_I^* \cdot \delta U_{rel}^{i-} \quad (82)$$

In order to get the insight of e_I , let be no oscillation prior to first impact, therefore

$$\delta U_{rel}^{i-} = 0 \quad (83)$$

Equation (82) is simplified to

$$U_{rel,s}^{1+} = (1-e_I^*) U_{rel,s}^{1-} \quad (84)$$

If (80) is examined one can find

$$\begin{aligned}
e_I &= \frac{\mu_{i,ef}}{m_{i,ef}} = \frac{m_2 m_3 (m_2 + m_3)^{-1}}{m_c m_t (m_c + m_t)^{-1}} = \frac{m_2 \cdot m_3 \cdot (m_c + m_t)}{m_c \cdot m_t \cdot (m_2 + m_3)} = \frac{m_2 \cdot m_3 \cdot (m_1 + m_2 + m_3 + m_4)}{(m_1 + m_2) \cdot (m_3 + m_4) \cdot (m_2 + m_3)} \\
&= \frac{m_1 m_2 m_3 + m_2^2 m_3 + m_2 m_3^2 + m_2 m_3 m_4}{m_1 m_2 m_3 + m_1 m_3^2 + m_1 m_2 m_4 + m_1 m_3 m_4 + m_2^2 m_3 + m_2 m_3^2 + m_2^2 m_4 + m_2 m_3 m_4} \Rightarrow \\
&\Rightarrow e_I = \frac{A}{A + m_1 \cdot m_3^2 + m_1 \cdot m_2 \cdot m_4 + m_1 \cdot m_3 \cdot m_4 + m_2^2 \cdot m_4} \leq 1 \quad (85) \\
&\text{where } A = m_1 \cdot m_2 \cdot m_3 + m_2^2 \cdot m_3 + m_2 \cdot m_3^2 + m_2 \cdot m_3 \cdot m_4 \\
&\text{and } m_1, m_2, m_3, m_4 \geq 0
\end{aligned}$$

Therefore one can deduce that

$$0 \leq e_I \leq 1 \quad (86)$$

and

$$0 \leq \mu_{i,ef} \leq m_{i,ef} \quad (87)$$

The coefficient e_I plays a significant role in determining whether the Chaser will continue, stop or change its direction of motion after an impact. This cannot be predicted using the simple rigid body theory, because this theory examines only the bodies under impact (in this case m_2 and m_3) without considering the mass ratio between the individual masses of the two multibody systems under impact (that is all the masses under consideration m_1, m_2, m_3 and m_4).

To examine the significance of the coefficient, assume a perfectly elastic impact occurs ($e^* = 1$) and using (81) and (84)

$$U_{rel,s}^{1+} = (1 - e_I^*) U_{rel,s}^{1-} = (1 - 2 \cdot e_I) U_{rel,s}^{1-} \quad (88)$$

Using (88), the following different generic cases can be identified:

- a) $e_I = 0 \Rightarrow U_{rel,s}^{1+} = U_{rel,s}^{1-}$: Retaining exactly the same velocity prior and after impact means that in fact, no impact has occurred in the first place. This is a limit case of ratio e_I .
- b) $e_I = 1 \Rightarrow \mu_{i,ef} = m_{i,ef} \Rightarrow U_{rel,s}^{1+} = -U_{rel,s}^{1-}$: This is another limit case of the ratio e_I . In fact it resembles an impact between 2 rigid bodies only. The relative velocity of the two systems becomes the relative velocity of two simple rigid bodies.

Both cases (a) and (b) are limit cases which prove the generality of the ratio of effective masses concept.

- c) $e_I = \frac{1}{2} \Rightarrow U_{rel,s}^{1+} = 0$: The CoM of the two multibody systems move at the same relative velocity after impact. In Sec. 4.3.1 this situation shall be further examined.
- d) $0 < e_I < \frac{1}{2} \Rightarrow U_{rel,s}^{1+} \cdot U_{rel,s}^{1-} > 0$: The CoM of the two multibody systems will have positive relative velocity after impact. Practically the Chaser will approach again the Target. This is a favourable situation during docking/ capture.
- e) $\frac{1}{2} < e_I < 1 \Rightarrow U_{rel,s}^{1+} \cdot U_{rel,s}^{1-} < 0$: The CoM of the two multibody systems will have negative relative velocity after impact. Practically the Target will fly away from the Chaser. This would prevent docking/ capture.

The above results prove additionally that the impact behaviour for the impact depends on the ratio of the masses, and not on the masses per se. This is in accordance with results presented in [84].

4.3.1 Further insights for e_I

It is interesting to examine the behaviour of e_I with respect to the ratio of masses between the bodies. For this reason the ratios between the masses are defined as

$$\lambda_c = \frac{m_2}{m_3} \quad \lambda_c = \frac{m_1}{m_2} \quad \lambda_t = \frac{m_4}{m_3} \quad (89)$$

therefore e_I becomes

$$\begin{aligned} e_I &= \frac{\mu_{i,ef}}{m_{i,ef}} = \frac{m_2 \cdot m_3}{m_2 + m_3} \cdot \frac{m_1 + m_2 + m_3 + m_4}{(m_1 + m_2) \cdot (m_3 + m_4)} \Rightarrow \\ &\Rightarrow e_I = \frac{((\lambda_c + 1) \cdot \lambda_t + (\lambda_t + 1))}{(\lambda_t + 1) \cdot (\lambda_c + 1) \cdot (\lambda_t + 1)} \end{aligned} \quad (90)$$

A number of plots were created for (90) using Mathematica. As it can be seen in **Figure 4-6** and **Figure 4-7**, large λ_c and λ_t are (i.e. more massive m_1 and m_4 respectively) have as a result the further approach of the Chaser to the Target (i.e. $e_I \leq 0.5$). However if m_2 and m_3 are prominent (i.e. λ_c and λ_t are reduced), the systems tend to reverse the relative velocity after impact (i.e. $e_I \geq 0.5$). In **Figure 4-8** one can deduce that as the mass of the Chaser becomes larger than the mass of the Target (because λ_c increases and λ_t remains constant) the systems tend after impact to retain an almost zero relative velocity (e_I tends to zero); however, as the Chaser has

analogous or lower mass than the Target, Chaser’s mass ratio plays critical role to the direction of the motion after impact. Similar explanations can be found in **Figure 4-9**, as the mass of the Chaser is larger than the mass of the Target (because λ_i increases and λ_c remains constant).

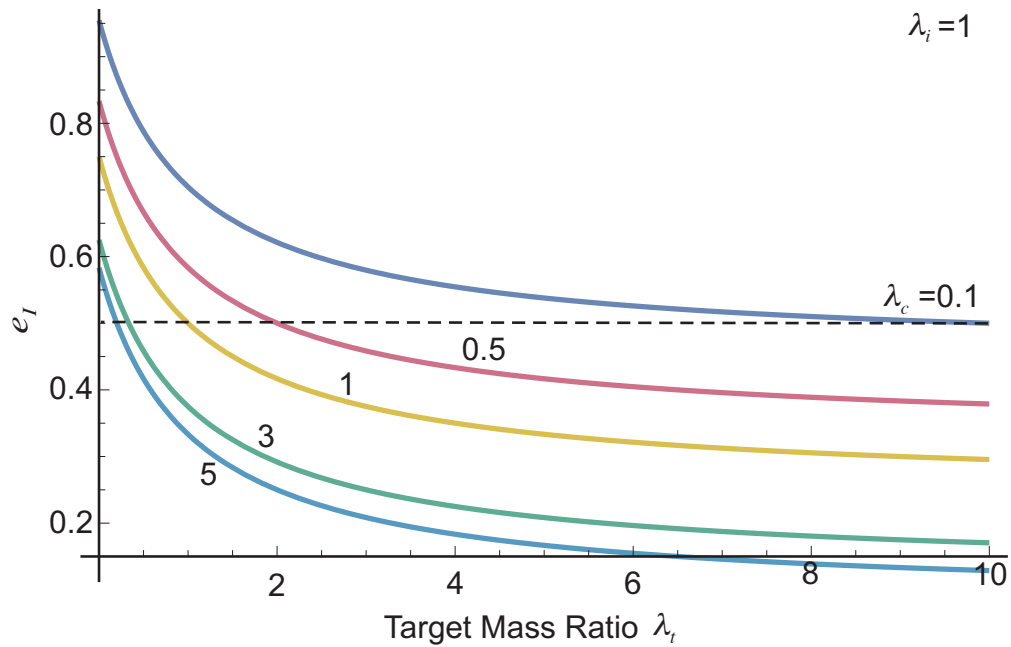


Figure 4-6. e_i vs Target’s mass ratio, for different Chaser mass ratios and $\lambda_i = 1$.

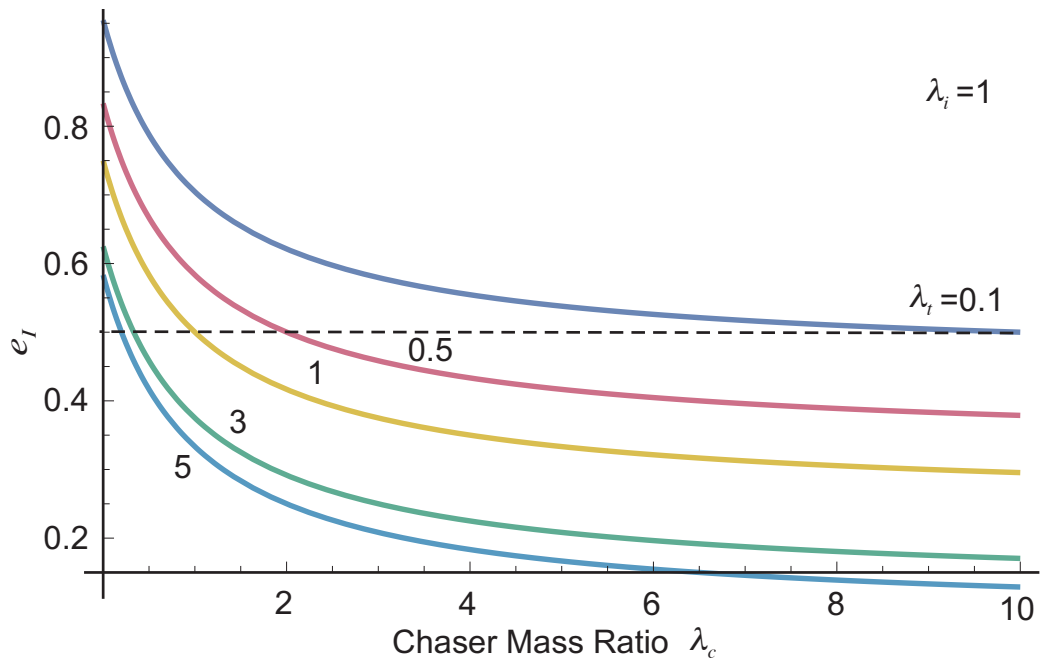


Figure 4-7. e_i vs Chaser’s mass ratio, for different Target mass ratios and $\lambda_i = 1$.

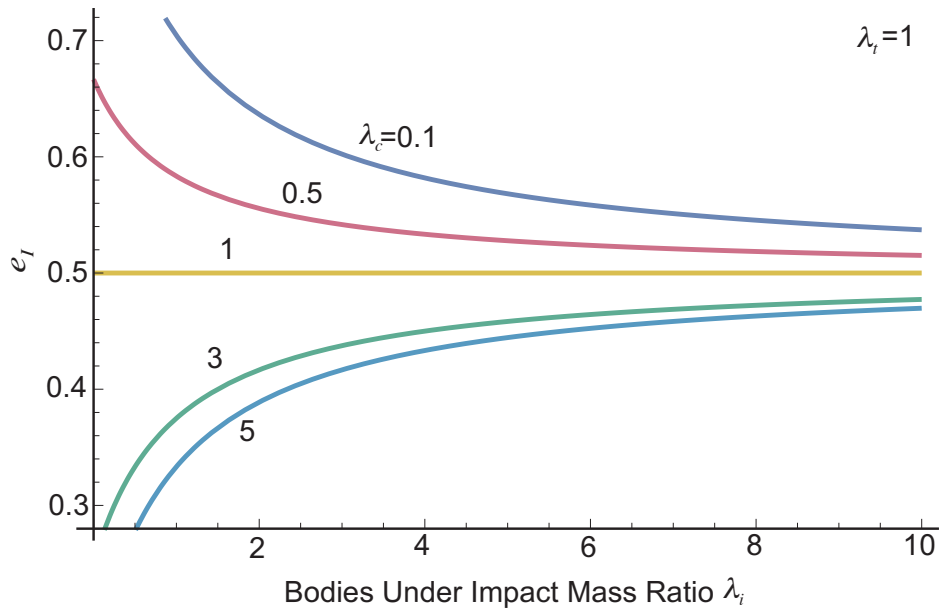


Figure 4-8. e_t vs masses under impact ratio, for different Chaser mass ratios and $\lambda_t = 1$.

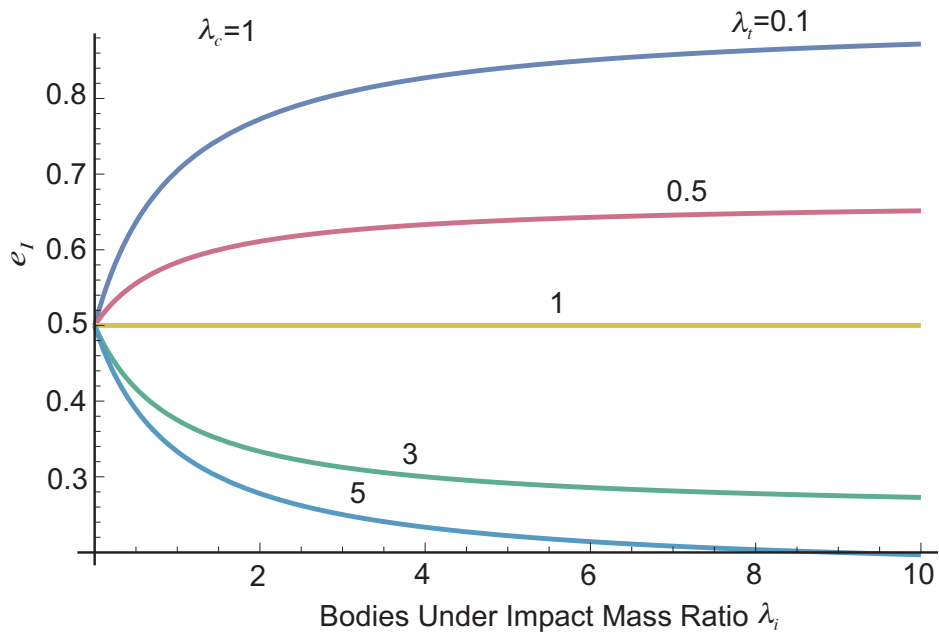


Figure 4-9. e_t vs masses under impact ratio, for different Target mass ratios and $\lambda_c = 1$.

Equal Mass Ratios of Chaser and Target

If one assumes that the ratios of the Chaser and the Target are equal (note that the absolute masses $m_1 - m_4$ and m_c, m_t are not required to be equal), that is

$$\lambda_c = \lambda_t = \lambda \tag{91}$$

so that (90) becomes,

$$e_I = \frac{1}{(\lambda+1)} \quad (92)$$

then using (81) and (84), one can find for the first impact

$$\begin{aligned} U_{rel,s}^{1+} &= (1 - (1 + e^*) \cdot e_I) \cdot U_{rel,s}^{1-} \Rightarrow \\ \Rightarrow U_{rel,s}^{1+} &= \left(1 - \frac{(1 + e^*)}{(\lambda + 1)}\right) \cdot U_{rel,s}^{1-} \Rightarrow \\ \Rightarrow U_{rel,s}^{1+} &= \left(\frac{\lambda - e^*}{\lambda + 1}\right) \cdot U_{rel,s}^{1-} \end{aligned} \quad (93)$$

The ratio λ can be only positive; therefore the numerator of (93) can be positive (and the systems will continue to move at the same direction because $U_{rel,s}^{1+} \cdot U_{rel,s}^{1-} > 0$) if and only if the ratio of the masses of the bodies λ , as in (91), is larger than the coefficient of restitution. Note however that $0 \leq e^* \leq 1$ therefore if $\lambda > 1$ then this situation is trivial because then $\lambda > e^*$ always. In other words (93) must be examined especially when the Target has larger m_2 than m_1 . Finally one can easily see that as the ratio λ increases, that is $m_1 \gg m_2$, the coefficient e_I tends to zero, therefore the Chaser keeps its direction after impact and the relative velocity of the systems is decreased partly.

Impact of three masses

In case either the Chaser or the Target cannot be modeled with more than one mass, then either $m_1 = 0$ or $m_4 = 0$. In this case $\lambda_c = 0$ or $\lambda_t = 0$ correspondingly. Let examine the case that the Target is one mass only. Using (90) one can find that

$$e_I = \frac{((\lambda_c + 1) \cdot \lambda_t + 1)}{(\lambda_t + 1) \cdot (\lambda_c + 1)} \quad (94)$$

Plotting this function, **Figure 4-10**, it can be seen that there is high tendency for the systems to change the direction of relative velocity (as $e_I > 0.5$) which is reasonable if it is considered that the whole energy of the impact of the Target is received only by one mass, and there is no spring or other mass to withstand the impulse. Therefore the only case that the systems retain their initial direction of relative velocity is in the case the Target is much more larger than the mass under impact from the side of the Chaser.

On the other hand if between the Chaser masses the spring is infinitely stiff or there is no flexibility, then (90) yields

$$e_I = \frac{1}{(\lambda_t + 1)} \quad (95)$$

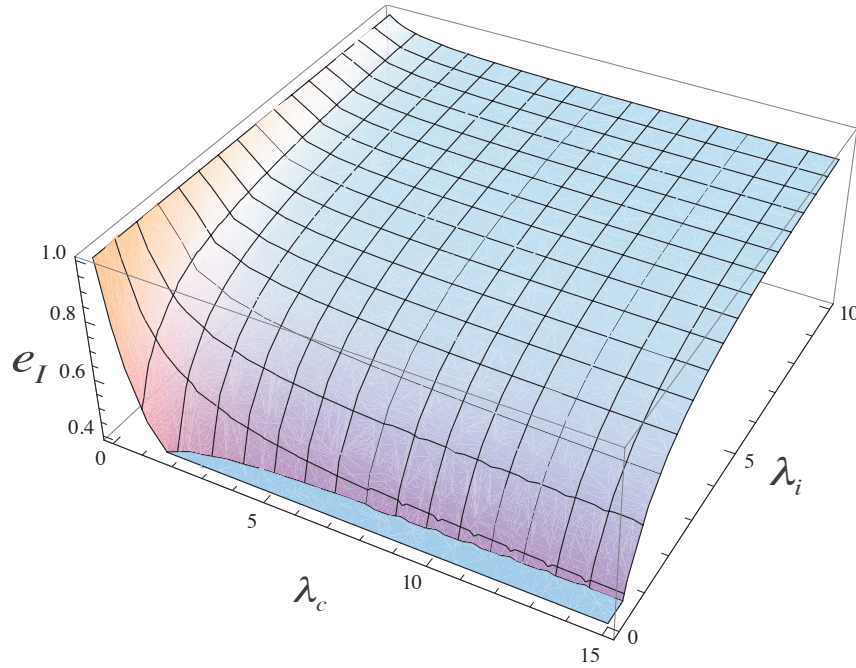


Figure 4-10. Impact of three masses, where the Target is only one mass.

Apparently (95) is similar to (92), with a different mass ratio. Thus, as the Chaser becomes larger it tends to retain its initial velocity.

Impact with a small mass connected to a very large mass

Another extreme case is when m_4 models a very large mass, like a fixed wall. Let $m_4 \rightarrow +\infty$.

This time it is better to solve again (90) and take into account that

$$m_4 \gg m_1, m_2, m_3 \quad (96)$$

which means that

$$\begin{aligned} e_I &= \frac{\mu_{i,ef}}{m_{i,ef}} = \frac{m_2 \cdot m_3}{m_2 + m_3} \cdot \frac{m_1 + m_2 + m_3 + m_4}{(m_1 + m_2) \cdot (m_3 + m_4)} \Rightarrow \\ \Rightarrow e_I &= \frac{m_2 \cdot m_3}{m_2 + m_3} \cdot \frac{m_4}{(m_1 + m_2) \cdot m_4} = \frac{m_2 \cdot m_3}{m_2 + m_3} \cdot \frac{1}{(m_1 + m_2)} \Rightarrow \\ &\Rightarrow e_I = \frac{\mu_{i,ef}}{(m_1 + m_2)} = \frac{\mu_{i,ef}}{m_c} \end{aligned} \quad (97)$$

By substituting the mass ratios from (89), it can be found that:

$$e_I = \frac{1}{(\lambda_i + 1) \cdot (\lambda_c + 1)} \quad (98)$$

In other words the larger the Chaser, the higher the relative velocity is, following an impact with respect to the relative velocity prior to the impact. Plotting this function, **Figure 4-11**, it can

be seen that after impact the systems in general retain the initial direction of the relative velocity, except in cases where the Chaser has a larger mass under impact and/or the mass connected to the wall has about the same mass as the Chaser.

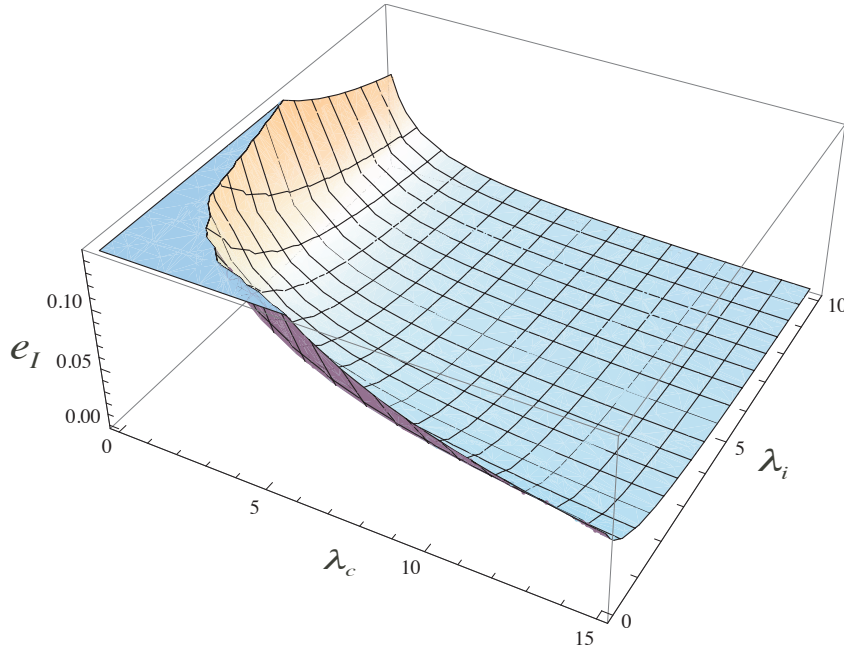


Figure 4-11. Impact with a Target which is comprised by a small mass connected to a very large mass.

Zero post-impact relative velocity

As **Figure 4-6** and **Figure 4-7** show, in some cases the relative velocity after impact can be zeroed ($e_I=0.5$) leading to a favourable situation. In fact, if this can be achieved, then the CoM of Chaser and the Target can assume zero relative velocity which is favourable to a space operation. In this case both systems will remain at a constant distance between; realistically this means that their relative velocity will be almost zero, thus the docking/ capture will exert lower reactions. Equating e_I in (90) with 0.5,

$$e_I = \frac{((\lambda_c + 1) \cdot \lambda_i + (\lambda_i + 1))}{(\lambda_i + 1) \cdot (\lambda_c + 1) \cdot (\lambda_i + 1)} = \frac{1}{2} \Rightarrow$$

$$\Rightarrow \lambda_c \cdot \lambda_i - \lambda_c \cdot \lambda_i \cdot \lambda_i + \lambda_i + \lambda_i - \lambda_c \cdot \lambda_i - \lambda_c - \lambda_i \cdot \lambda_i + 1 = 0$$
(99)

Three cases result:

- i. If $\lambda_c = c$ and known then,

$$\lambda_i \cdot (c + 1) \cdot (1 - \lambda_i) + (1 - c) \cdot (\lambda_i + 1) = 0$$
(100)

which is presented in **Figure 4-12**. As it can be seen, if the mass ratio of the Chaser is unity, $\lambda_c = 1$, then if the mass ratio of the Target is also unity, $\lambda_i = 1$, it does not matter what is the mass

ratio between the systems themselves. However in general, it is obvious that in order to find a relation of the mass ratios that would zero the post impact relative velocity, the following must apply as **Figure 4-12** shows: if the mass ratio of the Chaser is larger than one, then the mass ratio of the Target should be less than one, and vice versa.

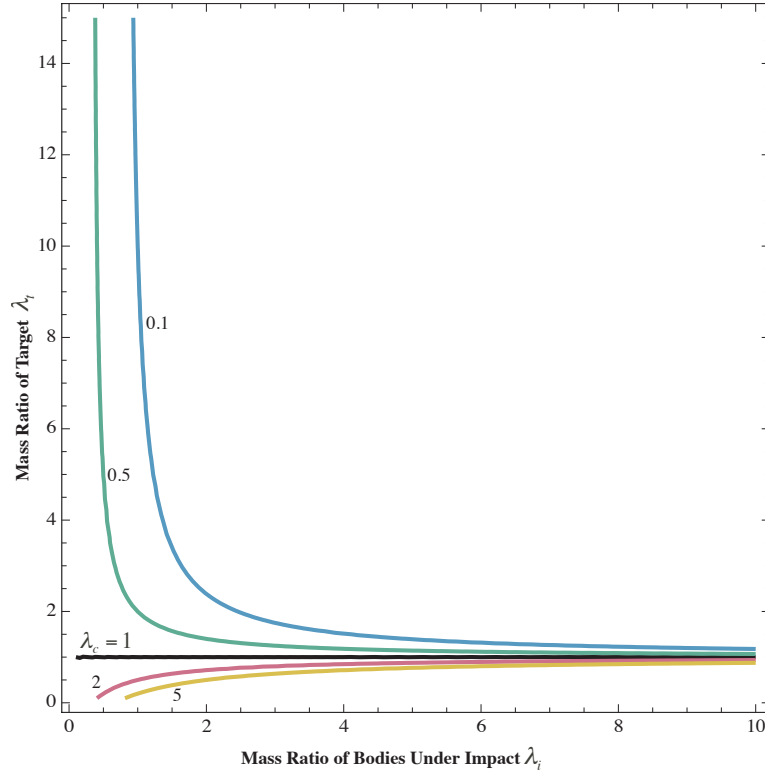


Figure 4-12. Mass ratio combinations which zero relative velocity after impact if the mass ratio of Chaser is known.

- ii. If $\lambda_t = c$ and known then,

$$(c-1) \cdot (\lambda_c - \lambda_t) + (1+c) \cdot (1 - \lambda_c \cdot \lambda_t) = 0 \quad (101)$$

which is presented in **Figure 4-13**. Again it is obvious that there is a qualitative reciprocity between the mass ratios of Chaser and Target.

- iii. If $\lambda_t = c$ and known then,

$$\lambda_i \cdot (1-c) \cdot (\lambda_c + 1) + (1+c) \cdot (1 - \lambda_c) = 0 \quad (102)$$

which leads to **Figure 4-14**. Qualitative reciprocity of the mass ratios between Chaser and Target is again evident. The results of the first case (Chaser mass ratio known) are also valid here.

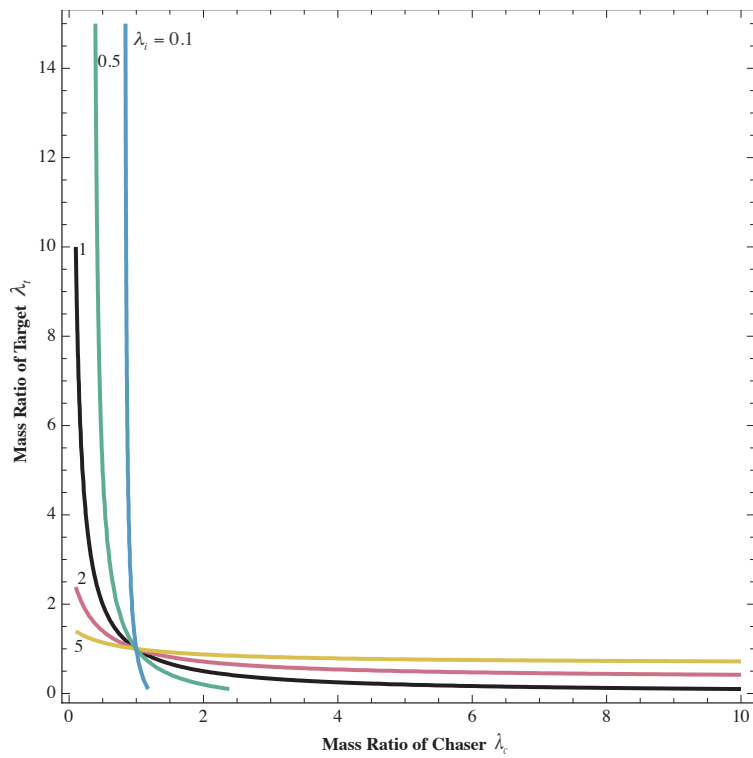


Figure 4-13. Mass ratio combinations which zero relative velocity after impact if the mass ratio of masses under impact is known.

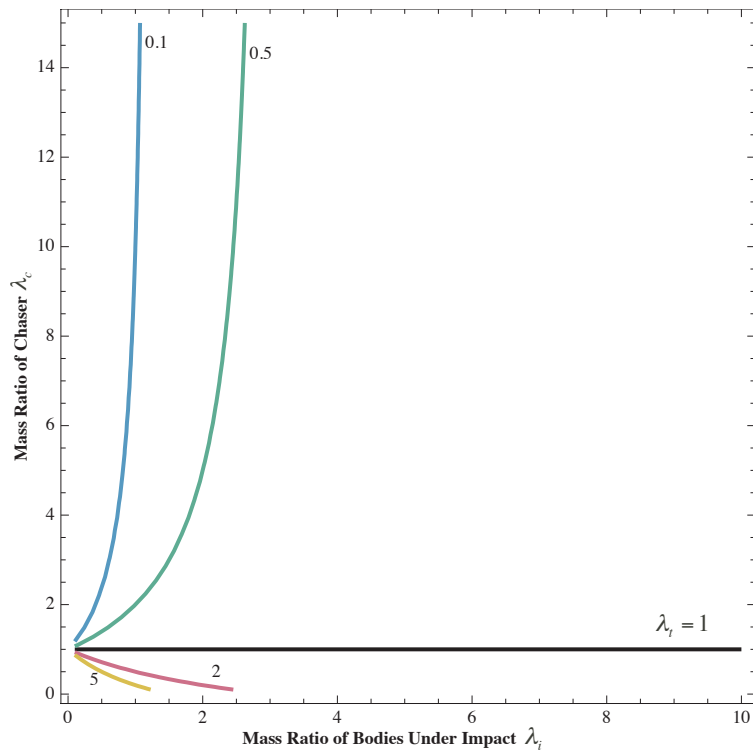


Figure 4-14. Mass ratio combinations which zero relative velocity after impact if the mass ratio of Target is known.

Varying Mass Ratios

In the next **Table 4-1**, the results of the previous analysis are summarized. In **Table 4-2** the special cases are also presented. Using this tables, a designer (of a system or a controller) will be able to assess the results of an impact between two multibody systems; it will be much faster to examine whether an impact will result in further approaching of the two multibody systems or not, and in case some parameters can be altered on-line, e.g. the compliance of appropriate joints in order to alter the ratio λ_c (see for example Sec. 4.2.3), then an impact which would lead to $e_I \rightarrow 0.5$ could be achieved, and thus a smaller tendency between the Chaser and Target to move apart after the impact.

Table 4-1. Effect of masses on the e_I .

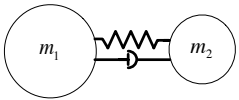
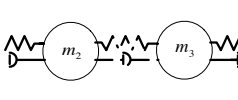
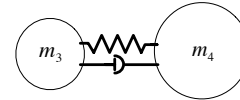
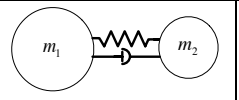
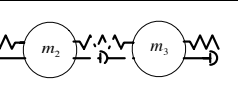
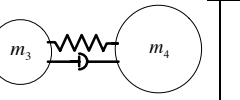
			e_I
Chaser	Bodies Under Impact	Target	
$m_1 \gg m_2$	$m_2 = m_3$	$m_4 \gg m_3$	Decrease
$m_1 \ll m_2$	$m_2 = m_3$	$m_4 \ll m_3$	Increase
$m_1 \ll \text{or} \gg m_2$	$m_2 \gg m_3$	$m_4 = m_3$	Tends to 0.5
$m_1 \gg m_2$	$m_2 \ll m_3$	$m_4 = m_3$	Decrease
$m_1 \ll m_2$	$m_2 \ll m_3$	$m_4 = m_3$	Increase
$m_1 = m_2$	$m_2 \gg m_3$	$m_4 \gg m_3$	Decrease
$m_1 = m_2$	$m_2 \gg m_3$	$m_4 \ll m_3$	Increase
$m_1 = m_2$	$m_2 \ll m_3$	$m_4 \ll \text{or} \gg m_3$	Tends to 0.5

Table 4-2. Calculation of e_I in special cases.

			e_I
Mass ratio for Chaser	Mass ratio for Bodies Under Impact	Mass ratio for Target	
λ	λ_i	λ	$\frac{1}{(\lambda+1)}$
0	λ_i	λ_i	$\frac{1}{(\lambda_i+1)}$

λ_c	λ_i	0	$\frac{((\lambda_c + 1) \cdot \lambda_i + 1)}{(\lambda_i + 1) \cdot (\lambda_c \cdot + 1)}$
λ_c	λ_i	$+\infty$	$\frac{1}{(\lambda_i + 1) \cdot (\lambda_c \cdot + 1)}$
c	λ_i	λ_i	0.5 if Eq. (100) applies
λ_c	c	λ_i	0.5 if Eq. (101) applies
λ_c	λ_i	c	0.5 if Eq. (102) applies

4.4 Discussion on Latching and Capture

4.4.1 Introduction of the latch concept

In this chapter a brief discussion on the latch concept and related issues will take place. As this is an ongoing work, this discussion aims on setting some insights on the challenges. Thus we study the case of a Chaser that must capture a Target, at a specific point, using a latch system. The question is whether this is possible for known systems and the challenges arise from the fact that both systems, the Chaser and the Target, are free floating systems. Additionally this procedure should be made without using any grasping system, that is the robotic arm of the Chaser should not use a grapple. The questions to be answered include:

1. How fast this operation should be made?
2. What is the relationship between the masses of the systems in order to achieve latching?
3. What is the relationship between the system stiffness and damping characteristics for a successful latch?

Latching in the Generic system

Let a system of two masses m (Target's latching Front End) and M (Target), which is at rest at the beginning of the procedure, see **Figure 4-15**. In order for the Chaser's probe to latch with the target in one impact, it must reach a point B selected by design; Point A is the point of free length of the spring, therefore the oscillation of m with respect to M will be around this point. Just after the impact m will move towards positive x-axis. While m is between points A and B, the probe cannot reach point B without impacting again m . While m is between points B and C, the probe should reach point B in order to latch. In other words, considering the oscillatory motion of m , in order for the probe to latch, the available time window is

$$0 \leq t_{Bmin} \leq T/4 \leq t_{Bmax} \leq T/2 \tag{103}$$

where T is the period of the oscillation of mass m , t_{Bmin} and t_{Bmax} is the minimum and maximum time respectively to achieve latching without having a new impact with m , during which would render the latching impossible, see also **Figure 4-16**. Minimum and maximum time also depend on the distance between points A and B, which is a design aspect. Note that in the presence of damping T is the damped periodic time.

According to (50) the maximum undamped elongation u_{max} of the spring is

$$u_{max} = \frac{P_i}{m \cdot \omega_0} \tag{104}$$

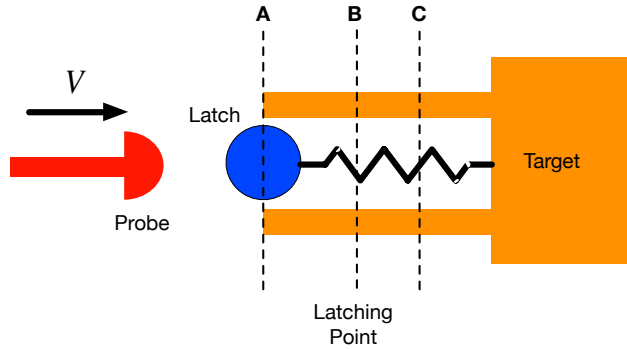


Figure 4-15. Characteristic points during motion of the latching system.

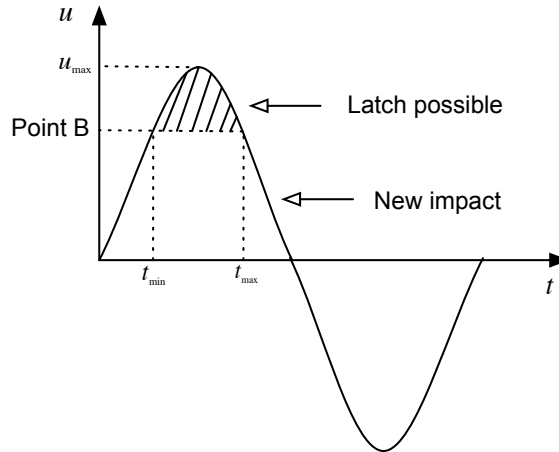


Figure 4-16. Time frame for possible latching.

therefore

$$u_B = u_{max} \cdot \exp(-\zeta \cdot \omega_0 \cdot t_B) \cdot \sin(\omega_0 \cdot t_B) \tag{105}$$

This equation should be solved for t_B . However (105) does not have an analytical solution, and should be solved numerically. As the damping factor tends to zero, the roots for t_B are

infinite; however only the first two roots are of interest to us, corresponding to the motion of the probe from A to C and back to A just after the first impact. On the other hand if the damping is ignored, one can find an analytical solution for (105), which is

$$t_{B\min} = \frac{1}{\omega} \cdot \arcsin\left(\frac{u_B}{u_{\max}}\right) \quad (106)$$

$$t_{B\max} = \pi - \frac{1}{\omega} \cdot \arcsin\left(\frac{u_B}{u_{\max}}\right) \quad (107)$$

Note however that the position B is a design parameter. In other words, the design characteristics of the probe, should be considered for the distance of point B

4.4.2 Requirements for Latching at First Impact

Introduction

In order to understand the requirements for latching at *first* impact, it is necessary to understand exactly the nature of the latching process. In this discussion it is essential to have two things in mind:

- i. Neither the Target nor the Chaser are fixed on a wall or on a floor. This situation has an instant implication: the impact cannot take a lot of time, because as the probe “pushes” the latch, it also “pushes” the CoM of the Target, and therefore a translational impulse which tends to “push away” the Chaser is getting larger. Strictly speaking, the integral of the impact force (impulse) from time 0 to time t_f when the impact ends, increases as t_f increases; thus the CoM of the Target is constantly accelerated during the impact duration.
- ii. During impact, by nature, the bodies under impact intend to move away one from each other, just immediately after the impact, except if another force pushes them back. This rule cannot be disregarded. In other words if two bodies come to an impact, a restitution phase will drive them away. The existence of another mass (in this work shown as m_1 for the Chaser and m_4 for the Target) connected with the masses under impact via lumped elements (springs and dampers) provide the inertia characteristics that prevent the total systems to initially move away from each other in some degree according to the parameters.

Let us now consider two extreme cases. First, let us assume that on the Chaser there is a manipulator, with a very soft end-effector. It is easy to imagine that even if the whole system has a large velocity, the required impulse to “push” the latch cannot develop (not enough impulse will be developed to force the latch and its spring to move for a predetermined distance). In the second case, consider a very stiff material at the End-Effector, but now the Chaser and/or the manipulator

is moving slowly. Again no impulse can be created to “push” enough the latch. The problem here is related with note (i) above: the larger the duration of the impact, the larger the impulse to the CoM of the Target, which tends to move further.

The previous mental pictures, point to the requirements for latch. In fact, the impact should be enough to “push” the latch past the latching point B, see again **Figure 4-15**. That is, the impulse to be created should be properly selected via the systems relative velocities. Secondly the post-impact velocities of the systems and the velocity of the probe must be such that the probe will reach the latching point B while (107) applies. That is the Chaser should be fast enough to reach the point before the Target gets away, and the probe should be faster than m_3 . In case one wishes the latch to be completed in a single impact, the probe should be faster than m_3 but not so fast, that result in reaching m_3 again before m_2 passes the latching point B.

Impulse and Maximum Elongation

The first requirement for a succesful impact is the maximum retraction (elongation) of the spring of the Target. This is directly connected with the developed impulse, which must be such that the maximum elongation is larger than the latching distance l_{latch} , see distance AB in **Figure 4-15**, which has been selected by the designer and incorporates the distance of the latching point on the Target and the size of the part of the probe which should pass the latching point. Apparently by choosing a maximum elongation near to the latching distance, one minimizes the time window when the latch could take place, still it is necessary as a reference number. Thus the requirement is

$$u_{\max} \geq l_{latch} \quad (108)$$

Using (104) one has

$$\begin{aligned} u_{\max} \geq l_{latch} &\Rightarrow \frac{P_i}{m_3 \cdot \omega_t} \cdot D_t \geq l_{latch} \Rightarrow \frac{(1+e^*) \cdot U_{rel,j}^i \cdot \mu_i}{m_3 \cdot \omega_t} \cdot D_t \geq l_{latch} \Rightarrow \\ &\Rightarrow U_{rel,j}^i \geq \frac{m_3 \cdot \omega_t \cdot l_{latch}}{(1+e^*) \cdot \mu_i} \cdot \frac{1}{D_t} = \frac{m_3 \cdot l_{latch}}{(1+e^*) \cdot \mu_{imp}} \cdot \sqrt{\frac{k_t}{\mu_t}} \cdot \frac{1}{D_t} \end{aligned} \quad (109)$$

Note that e^* refers to the coefficient of restitution between the bodies under impact and D_t to the internal damping characteristics between the masses of the Target. Apparently, the larger the latching distance l_{latch} , the Target's mass under impact or the stiffness of the Target's spring are, the higher impact velocity is necessary. On the other hand as e^* and D_t decrease, the impact velocity should be increased further. This is reasonable and in accordance to experience.

Example

Let a Chaser and a Target with the following characteristics:

$$\begin{aligned} m_1 &= 100kg, m_2 = 10kg, m_3 = 1kg, m_4 = 10kg \\ K_i &= 1000N/m, U_{rel\ i}^1 = 0.05m/s, c = 0, e^* = 0.9 \end{aligned} \quad (110)$$

What should be the latching distance to achieve latching? Interestingly if (109) is being used, one can find that

$$l_{latch} \leq 0.0026m \quad (111)$$

which means that the latching distance cannot be greater than 2.6mm in this case. However suppose that the latching distance is 0.01m. Using (109) again it can be found that the initial relative velocity should be $0.192m/s$, which is a speed higher than the usual speeds during the final phase of a docking operation. A very robust controller is needed to perform this operation with great accuracy. This example points the difficulties of latching in free-floating systems.

4.5 Verification in MATLAB/Simulink

4.5.1 Description of Simulations

In order to verify the proposed RMIT theory, a MATLAB/ Simulink model has been created. To test the validity of the propositions, the model is fully analytical. Each system (Chaser and Target) has been modeled as a 2-mass spring-damper system. The contact forces between the bodies under impact are calculated using the KV model (for simplification of the process). In particular the impact is modelled by a spring-damper system which can only be compressed. As the simulation advances, Simulink calculates the velocities of the masses under impact, and their interpenetration. This interpenetration feeds the contact model and a force is developed which pushes away the masses under impact. Therefore prior and after the impact, the simulation presents two 2-body systems, and during impact a 4-body system. No equation stemming from the proposed RMIT was used to obtain independent results. Thus the validity of the proposed theory is examined via a complete visco-elastic theoretical formulation.

In the Simulink blocks, see **Appendix B**, the user can set the magnitude of all masses, the initial velocity of the Chaser (the Target is assumed still with respect to the Chaser at the start of the simulation, without loss of generality), and the stiffness and damping coefficients of all springs and dampers, including the contact stiffness and damping, according to the impact model (i.e. here KV). The user can also change other initial parameters of the bodies, however, except for the initial velocity of the Chaser (m_1 and m_2 have the same velocity, therefore the internal spring and damper of the Chaser produce no internal forces at the beginning of each simulation run) and its initial position, all other values are set to zero.

4.5.2 Verification of RMIT

In order to verify the theoretical calculations of post-impact relative velocity between Chaser and Target, in relation to the pre-impact corresponding velocity, various configurations were examined. All simulations proved the validity of the proposed theory. In the runs, the masses considered were: A) the masses of the robotic systems of the CSL emulator, B) All masses equal and C) and D) random masses. **Table 4-3** presents these values and the calculations according to (84). **Figure 4-17** shows the relative velocities of all cases. Only the first impact (which is of interest) is shown for each example. It can be seen that in all cases the theoretical model finds the post-impact relative velocity with high accuracy. Note that the stiffnesses have been selected low in order to obtain clearer plots; however with higher stiffnesses the results are the same, and the only difference is the duration of the impact. Note that only the relative magnitude of the system's stiffnesses with respect to the contact stiffness is of interest. The damping was set to zero, in order to examine the validity of the RMIT proposition in elastic impacts.

Table 4-3. Data and results of the first set of simulations.

Property	Example A	Example B	Example C	Example D
m_1 (kg)	17	10	5	100
m_2 (kg)	2	10	50	20
m_3 (kg)	1.5	10	10	10
m_4 (kg)	15	10	100	200
Contact Stiffness (N/m)	1000	1000	1000	1000
Chaser Stiffness (N/m)	15000	15000	15000	15000
Target Stiffness (N/m)	200	200	200	200
Initial Rel. Velocity (m/s)	0.05	0.05	0.05	0.05
Final Rel. Velocity (Eq. 33) (m/s)	0.0403	0	0.02728	0.0413
Final Rel. Velocity (sim) (m/s)	0.0402	-0.000476	0.02715	0.0412
Absolute Error (m/s)	0.0001	0.000476	0.00013	0.0001
Relative Error (%)	0.25	-	0.48	0.24

Another interesting comparison, Examples E1-E3, is obtained by using the same masses, but with different stiffnesses. As shown in **Figure 4-18**, the duration of the impacts change (which is reasonable) but not the final value of the relative velocity of the systems after impact. The full sequence of impacts is not presented.

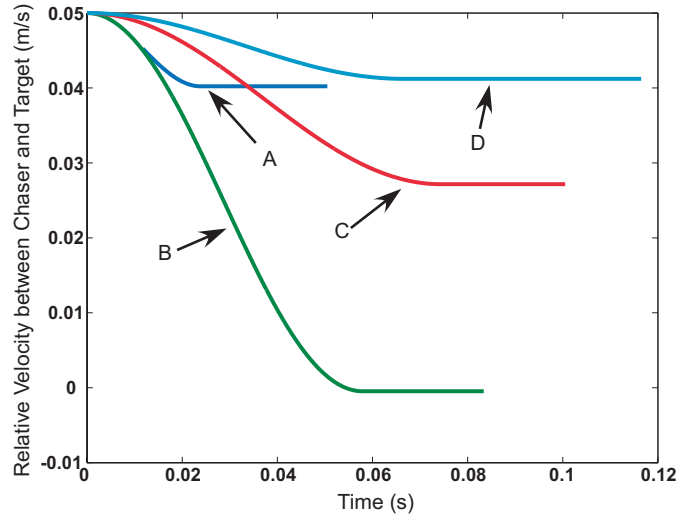


Figure 4-17. Relative velocities between Chaser and Target after first impact. Examples A-D.

Another limiting case is presented, Example F. It resembles a small chaser consisting of two equal small masses, which hits a wall of (practically) infinite mass (the last mass m_4 is used only to avoid zeroing the denominator in simulations). According to the theory, the relative velocity for the first impact should be close to zero for an elastic impact (thus no the coefficient of restitution is unity). This is confirmed (an error is expected due to round-off errors), **Figure 4-19**.

Table 4-4. Data and results of the second set of simulations.

Property	Example E1	Example E2	Example E3	Example F
m_1 (kg)	17	17	17	10
m_2 (kg)	2	2	2	10
m_3 (kg)	1.5	1.5	1.5	10000000
m_4 (kg)	15	15	15	1
Contact Stiffness (N/m)	10	100	10000	1000
Chaser Stiffness (N/m)	150	15000	1500000	15000
Target Stiffness (N/m)	2	20	2000	500
Initial Rel. Velocity (m/s)	0.05	0.05	0.05	0.05
Final Rel. Vel. (Eq. 33) (m/s)	0.0403	0.0403	0.0403	0
Final Rel. Velocity (sim) (m/s)	0.0402	0.04029	0.04029	-0.00167
Absolute Error (m/s)	0.0001	0.00001	0.00001	-0.00167
Relative Error (%)	0.25	0.025	0.025	-

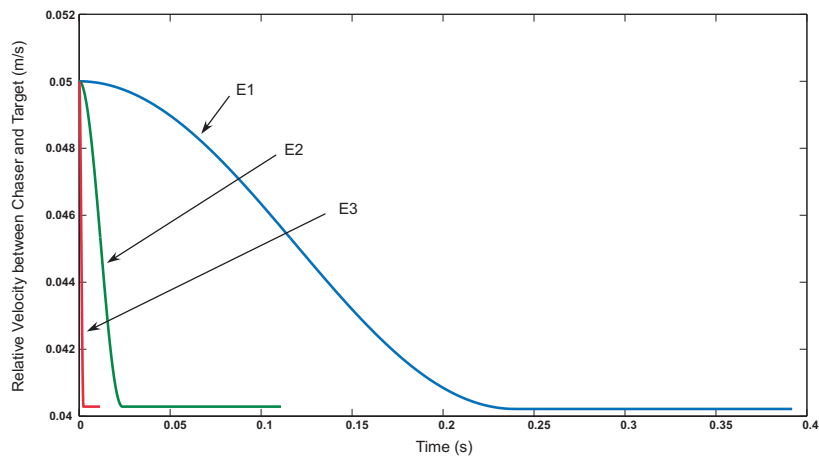


Figure 4-18. Relative velocities between Chaser and Target after first impact. Examples E.

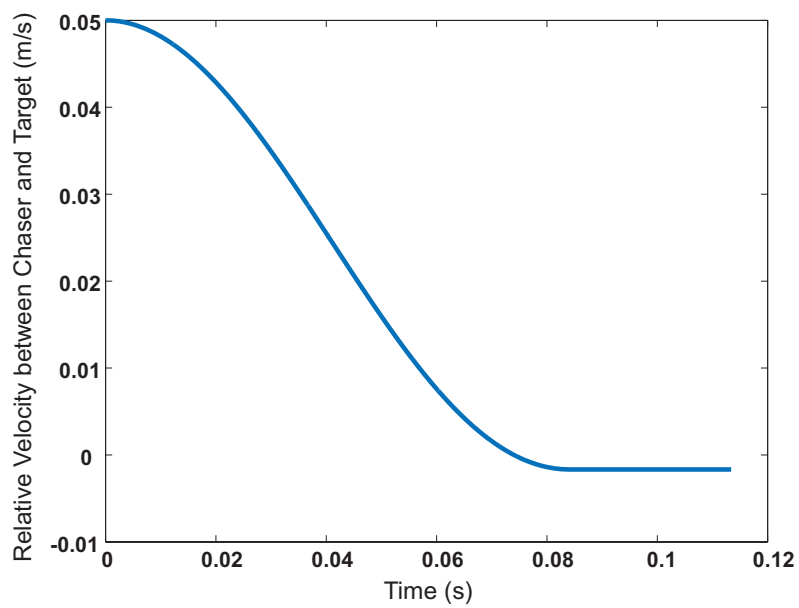


Figure 4-19. Relative velocity between Chaser and Target after first impact. Example F.

